

# **SILVER NANOPARTICLE LOADED MICROEMULSION FOR CANCER THERAPY**

Thesis Submitted For the Award of the Degree of

**DOCTOR OF PHILOSOPHY**

**(PHARMACEUTICAL SCIENCES)**

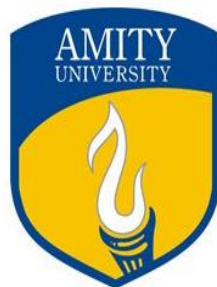
By

**Ms. ANUPAMA**

Under the Supervision of

**Dr. AMRISH CHANDRA**

**Prof. (Dr.) ROOP KRISHEN KHAR**



**AMITY INSTITUTE OF PHARMACY, NOIDA**

**AMITY UNIVERSITY, UTTAR PRADESH**

**INDIA**

**201313**

## **CHAPTER-6**

### **RESULTS AND DISCUSSION**

#### **1 Preformulation study of Gallic acid**

Preformulation studies characterize physical and chemical properties of drug to develop safe, effective and stable dosage form. Table 6.1 presents the results of Preformulation studies of Gallic acid.

Table 6.1 *Preformulation Study of Gallic acid. Data was Presented as Mean ± SD (n=3)*

Organoleptic properties		Meltin g point	Solubility		Partition coefficie nt	pH
			Solvent	solutibilit y		
Color	White to off white crystallin e solid	260 <sup>0</sup> C± 0.012	Distilled water	Slightly soluble	0.70±0.21 0.60±0.11	3.22±0 .25
Odor	Odorless		Methanol	Freely Soluble		
Description	Crystalline		Ethyl alcohol	Soluble		
Taste	Slightly bitter		Acetone	Freely Soluble		
			Chlorofor m	Sparingly soluble		
			Benzene	Slightly soluble		
			pH 7.4±1	Freely Soluble		
			pH 5±1	Freely Soluble		

### **1.1 Determination of solubility**

Different solvents were used to determine the solubility of GA are presented in Table 6.1. The maximum solubility was observed in PBS Ph 7.4, acetate buffer pH 5, water, ethanol and acetone and least in benzene.

### **1.2 Determination of partition coefficients**

Partition coefficient is an important factor in designing formulations in purpose of absorption of drug from an aqueous environment to the lipophilic membrane. For oral absorption of the permeant (octanol/phosphate buffer) the partition coefficient must be in the range of -0.4 to +5.6 range. The responses of the partition coefficient analysis are presented in Table 6.1 where the values of partition coefficient were found in octanol/Phosphate buffer and acetate buffer is  $0.70 \pm 0.21$  and  $0.60 \pm 0.11$  respectively. The results revealed the lipophilic nature of formulation and is suitable for designing formulations for oral application.

### **1.3 Melting point (MP) and pH determination**

MP of pure GA was found  $260^{\circ}\text{C} \pm 0.012$  was presented in Table 6.1 which is close to the standard value  $258\text{-}265^{\circ}\text{C}$ . The observed value of MP indicates the purity and identification of GA. The pH of Gallic acid was found  $3.22 \pm 0.25$  (Table 6.1) which is near to the standard value 3.20 (Badhani et al., 2015).

### **1.4 Identification of absorption maxima ( $\lambda_{\text{max}}$ ) of Gallic acid**

The  $\lambda_{\text{max}}$  for quantitative analysis of GA was determined after scanning the appropriate dilute solution between 200-800 nm using UV-Vis and in pH 7.4 and pH 5 buffer was found to be 270 and 268 nm respectively as presented in Figure 6.1.

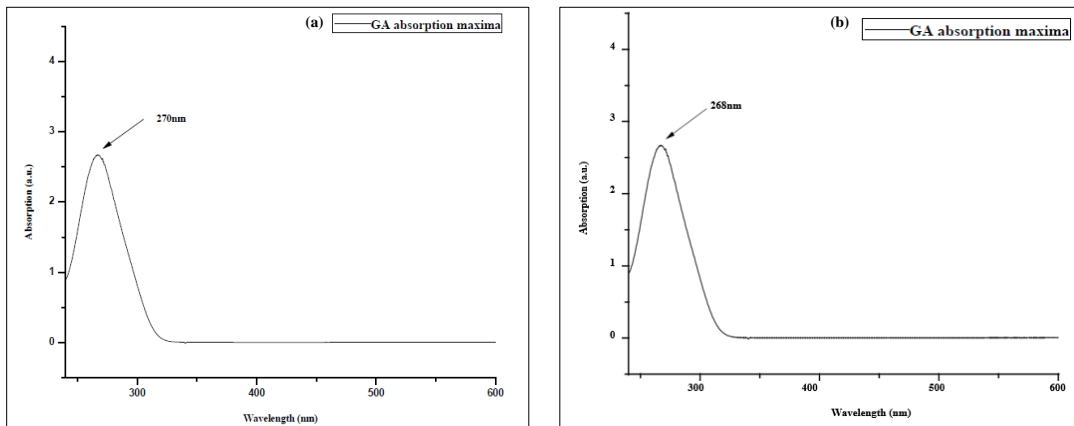


Figure 6.1. Determination of absorbance maxima ( $\lambda_{\text{max}}$ ) in (a) pH 7.4 and (b) pH 5 buffer.

### 1.5 Standard plot of Gallic acid

The standard curves of Gallic acid were prepared in pH 7.4 and pH 5 buffering solution within the concentration range of 10-50  $\mu\text{g/ml}$  were presented in Figure 6.2 and Figure 6.3 respectively. A straight line found with regression coefficient ( $R^2$ ) = 0.9998 and 0.9991 value in pH 7.4 and pH 5 respectively which indicates that drug follows Beer's law.

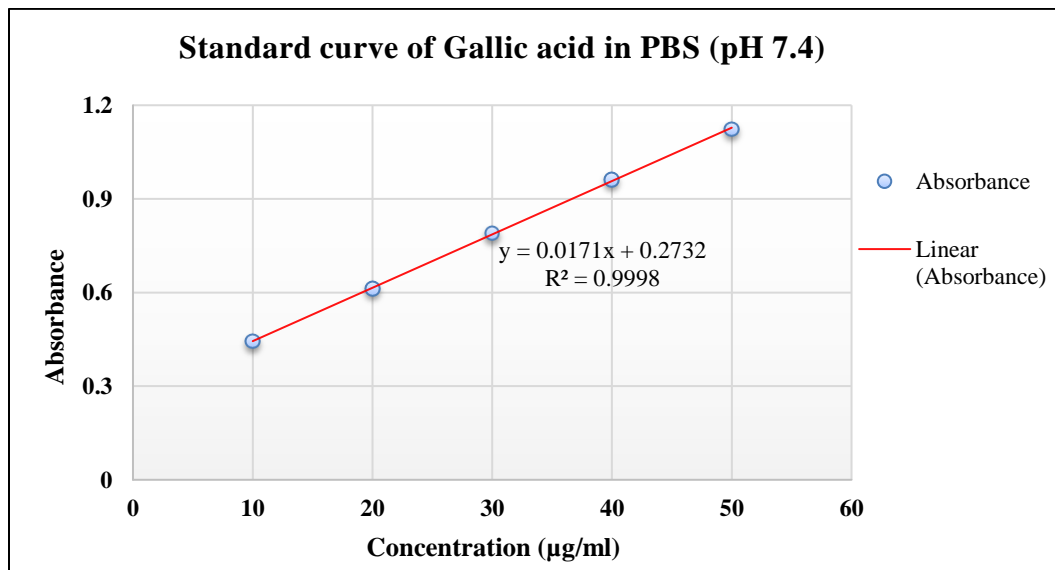


Figure 6.2. Standard plot of Gallic acid in PBS (pH 7.4) at  $\lambda_{\text{max}}$  270 nm.

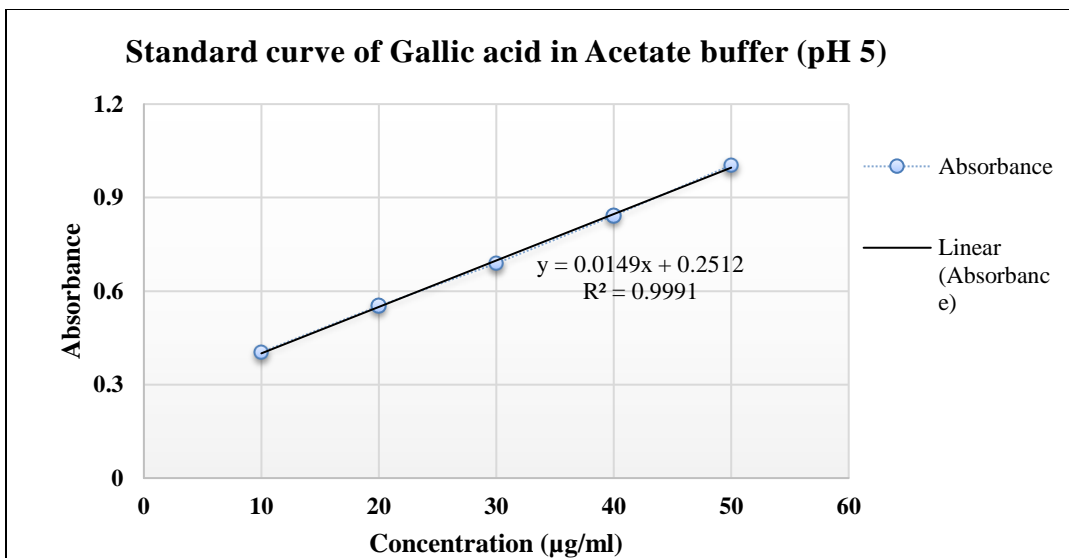
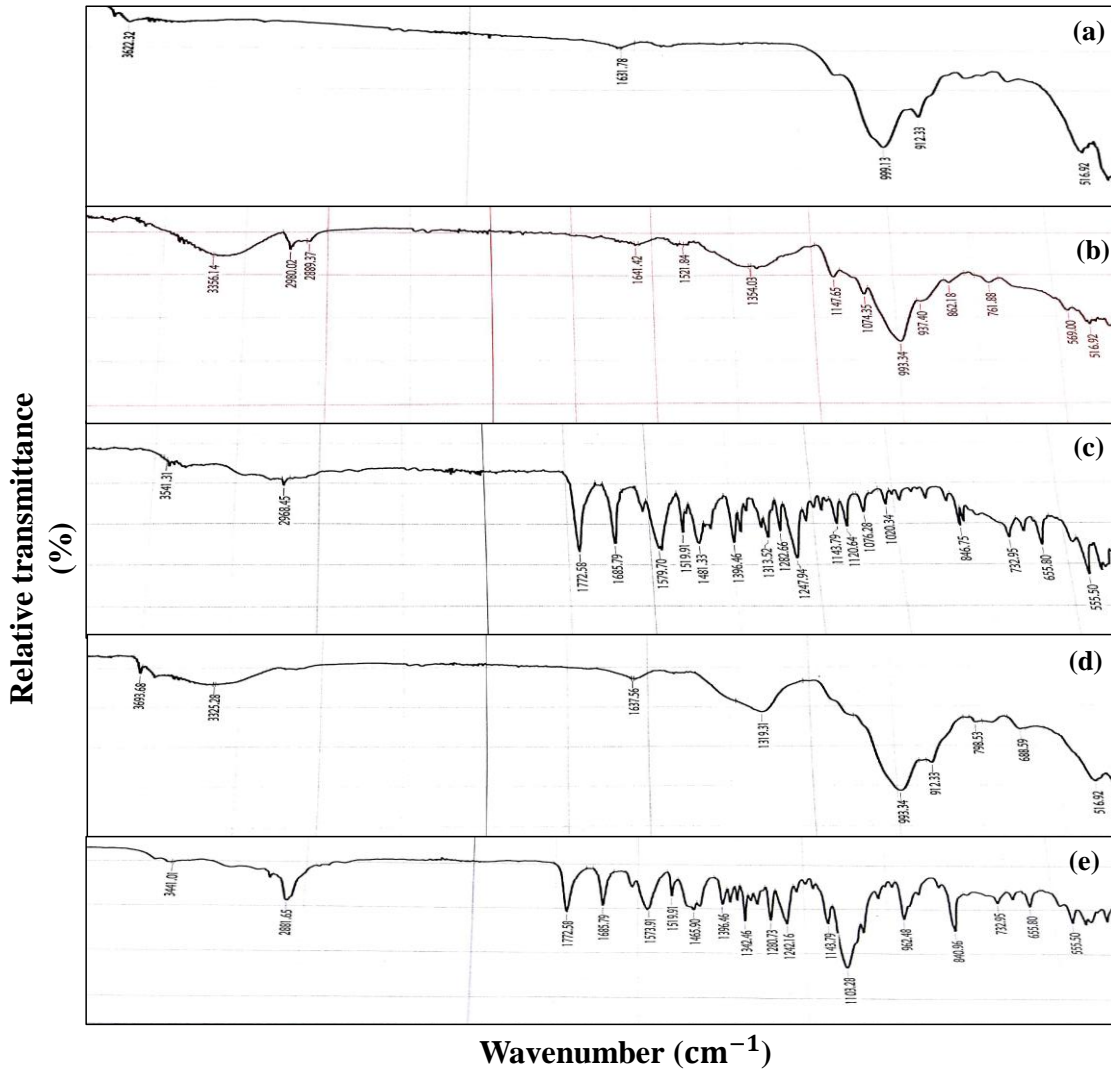


Figure 6.3. Standard plot of Gallic acid in Acetate buffer (pH 5) at  $\lambda_{\text{max}}$  268 nm.

## 2 Drug-Excipients interaction studies

FTIR spectroscopy is used for identifying functional groups of GA, bentonite, starch and AgNPs or possible molecules which define the mechanism of silver ions reduction and any interaction (Thapliyal & Chandra, 2018)(Theivasanthi & Alagar, 2013a). The FTIR graph of bentonite in Figure 6.4a presented the bands at  $3622\text{ cm}^{-1}$  due to vibration for stretching of OH, at  $1631\text{ cm}^{-1}$  due to bending of H-O-H bond, at  $993\text{ cm}^{-1}$  due to stretching of Si-O, at  $630\text{ cm}^{-1}$  because of stretching of Al-O-H, at  $912\text{ cm}^{-1}$  vibration because of (Al, Mg-O-H) and at  $516\text{ cm}^{-1}$  due to bending of Si-O-H (Thapliyal & Chandra, 2018)(Alemdar, Gungor, Ece, & Atici, 2005). Figure 6.4b presents the IR spectra of starch biopolymer which showed the peak at  $3356\text{ cm}^{-1}$  due to O-H stretching vibration and at  $1641.42\text{ cm}^{-1}$  due to the presence of amide group. Figure 6.4c indicates a broadband peak between  $3552$  and  $2510\text{ cm}^{-1}$  and the sharp-edge peak at  $1772\text{ cm}^{-1}$  due to the vibration of O-H (alcohol) group and a C-O stretching, which confirms the presence of carboxyl group in the GA. This carboxyl group binds to the surface of the AgNPs (Thapliyal & Chandra, 2018). These bonds disappeared after the synthesis. The absorption peak recorded at  $1685$ ,  $1579$ ,  $1571$  and  $1481\text{ cm}^{-1}$  was subjected for vibration stretch of C-C bonds in an aromatic group(W. Wang et al., 2007a). Various peaks observed in  $1313$ – $1020\text{ cm}^{-1}$  region corresponded to vibration of C–O stretch bond and O–H bond of bending vibration of phenolic GA (W. Wang et al., 2007a). The combination peaks present due to bentonite and the amine groups of starch confirmed in the spectrum of Ag/bentonite/starch

composites (Figure 6.4d). The peaks of hydroxyl (O-H) groups is little adjusted towards lowering the wave numbers in 3441 from 3693 $\text{cm}^{-1}$  in bentonite and BNCs (W. Wang et al., 2007a). The FTIR spectra of AgNPs (Figure 6.4e) indicate that the carbon-hydrogen (C-H) and amine (-NH<sub>2</sub>) peaks of GA were shifted to 2881, 1573, and 1465  $\text{cm}^{-1}$  from 2968, 1685, and 1579  $\text{cm}^{-1}$  which confirms the deformation of the amine group of starch. Various peaks of high and low wave numbers present due to the connection between the bentonite's silicate layers and starch. The aliphatic C=H stretching sharp peak corresponds to the wave number 2881  $\text{cm}^{-1}$  and C=C peak at 1685  $\text{cm}^{-1}$  due to stretching vibration. These peaks indicate the presence of alcohol and alkene groups in the GA may be involved in the reduction process to synthesize AgNPs which overlap starch peaks in 1637 and 1612  $\text{cm}^{-1}$  with a bentonite peak in 1631  $\text{cm}^{-1}$ . The peaks present in wave number 1465.90, 1396.46, and 1342.46  $\text{cm}^{-1}$  due to bending vibration of C-H, like the GA peaks. Various large peaks were observed corresponds to the O-H, amine, and C-H bending groups of GA on the synthesized AgNPs formulation (W. Wang et al., 2007a) as depicted in Figure 6.4e. The observation of presented bands confirm that due to the existence of various complex peaks between the groups and AgNPs in the Ag/bentonite/GA BNCs, the observed peaks are little adjusted toward the lower wave numbers with enhanced intensity (Shameli et al., 2011c). The spectrum of Ag/GA/starch/bentonite composite (Figure 6.4e) showed a shift of the GA peaks in 1685 and 1579 to 1685 and 1573  $\text{cm}^{-1}$ , respectively. The peak of 1396  $\text{cm}^{-1}$  due to vibration of Ag/GA determines the reduction mechanism of silver using GA due to interaction between them. The FTIR graph of Ag/starch/bentonite nanocomposites (Figure 6.4d) indicates a narrow peak of O–H group presented at 3441  $\text{cm}^{-1}$  due to vibration compared to Ag/GA/starch/bentonite nanocomposite (Figure 6.4e). The above results confirm that the chemical bond exists between GA molecules and Ag nanoparticles and compatibility between GA and other excipients mixtures.



*Figure 6.4.* FTIR graph of (a) Bentonite, (b) Starch, (c) Gallic acid, (d) Excipients mixture; Ag/Bentonite/Starch composite and (e) Drug excipients mixture; Ag/Bentonite/Starch/GA.

### 3. Synthesis of AgNPs in Bio-nanocomposites (BNCs)

Silver NPs synthesized in bio-nanocomposites using green reduction by Gallic acid.

#### 3.1 Artificial neural network model

In this research, AgNPs optimized using the NN model applied with software tool of neural network technique in MATLAB 2013 version. It is applied to evaluate the connection between 4 input factors such as concentration of  $\text{AgNO}_3$  in Molar, weight % of starch, amount of Bentonite in g and concentration of GA in Molar and response factor of the nanometer size of AgNPs, as depicted in Figure 6.5.

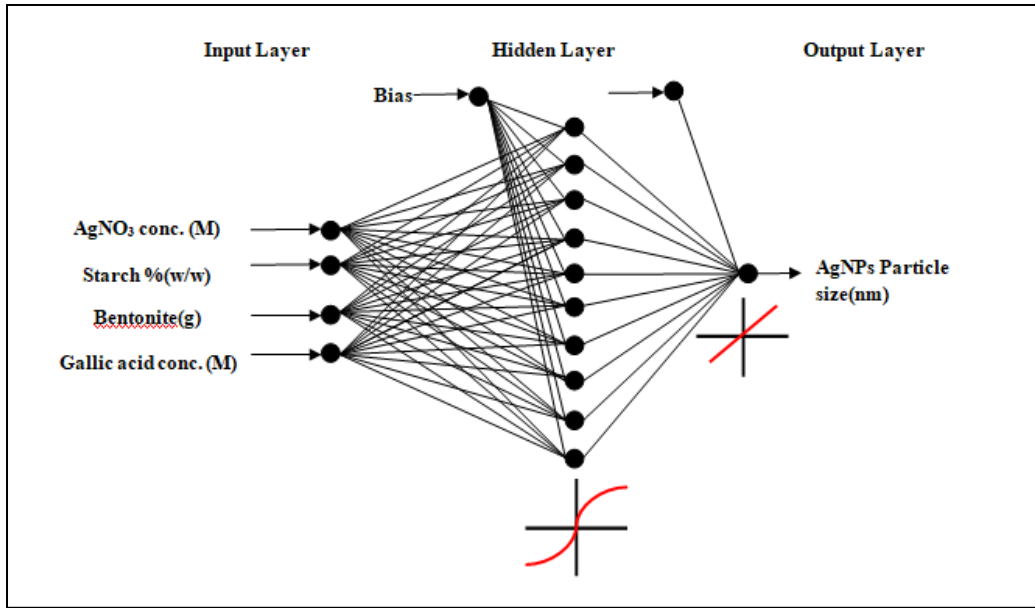


*Figure 6.5.* Diagrammatic representation of ANN model determining the relationship between formulation and response variables (AgNPs particle size).

The different concentration of formulation variables examined for the providing the best fit NN model depicted in Table 6.2. This table represents the 4 experimental factors with 1 response factor and illustrates the interconnection mechanism between them in response to the selected range of response values. Error between the predicted and actual NPs size was determined based on their differences. The formulation with minimum absolute error was found the best formulation.

Table 6.2 *Different Concentration of Experimental Variables with Respect to ANN model Predicted Response Variables (AgNPs size)*

Ru n no.	AgNO <sub>3</sub> Con. (Molar )	Starc h (g)	Bentonite amount (gram)	GA (Molar )	AgNPs experimental size (nm)	AgNPs predicted size (nm)	Absolute Error (nm)= experimental -predicted
1	1×10 <sup>-3</sup>	5×10 <sup>-4</sup>	3×10 <sup>-3</sup>	4×10 <sup>-3</sup>	68.060	68.061	-0.001
2	1×10 <sup>-3</sup>	5×10 <sup>-4</sup>	5×10 <sup>-3</sup>	4×10 <sup>-3</sup>	68.070	68.080	-0.010
3	1×10 <sup>-2</sup>	5×10 <sup>-3</sup>	4×10 <sup>-2</sup>	4×10 <sup>-2</sup>	68.900	68.886	0.014
4	1×10 <sup>-2</sup>	5×10 <sup>-3</sup>	8×10 <sup>-2</sup>	4×10 <sup>-2</sup>	68.910	68.691	0.219
5	1×10 <sup>-1</sup>	5×10 <sup>-2</sup>	0.032×10 <sup>1</sup>	4×10 <sup>-1</sup>	78.820	78.904	-0.084
6	1×10 <sup>-1</sup>	5×10 <sup>-2</sup>	0.036×10 <sup>1</sup>	4×10 <sup>-1</sup>	78.830	78.750	0.080
7	2×10 <sup>-1</sup>	1×10 <sup>-1</sup>	0.063×10 <sup>1</sup>	8×10 <sup>-1</sup>	82.930	82.935	-0.005
8	2×10 <sup>-1</sup>	1×10 <sup>-1</sup>	0.065×10 <sup>1</sup>	8×10 <sup>-1</sup>	82.950	82.980	-0.030
9	3×10 <sup>-1</sup>	15×10 <sup>-2</sup>	0.092×10 <sup>1</sup>	12×10 <sup>-1</sup>	89.100	89.077	0.023
10	3×10 <sup>-1</sup>	15×10 <sup>-2</sup>	0.096×10 <sup>1</sup>	12×10 <sup>-1</sup>	89.500	89.506	-0.006
11	4×10 <sup>-1</sup>	2×10 <sup>-1</sup>	0.0121×10 <sup>2</sup>	16×10 <sup>-1</sup>	92.600	92.610	-0.010
12	4×10 <sup>-1</sup>	2×10 <sup>-1</sup>	0.0127×10 <sup>2</sup>	16×10 <sup>-1</sup>	93.400	93.150	0.250
13	5×10 <sup>-1</sup>	25×10 <sup>-2</sup>	0.0152×10 <sup>2</sup>	20×10 <sup>-1</sup>	105.710	105.699	0.011
14	5×10 <sup>-1</sup>	25×10 <sup>-2</sup>	0.0155×10 <sup>2</sup>	20×10 <sup>-1</sup>	105.900	106.004	-0.104

For efficient functioning of NN model, data samples was categorized in a simple random way due to its easy to implement (Thapliyal et al., 2018). The 14 sample data of experimental factors were divided into three parts (70, 15, and 15% respectively) with 10 samples for training, 2 for testing and 2 for validation based using MATLAB software (Thapliyal et al., 2018)(Shabanzadeh et al., 2015c). This is expressed as “early stopping”

that is used to prevent the model from overfitting of sample data sets (Thapliyal et al., 2018)(Shabanzadeh et al., 2015c)(Shabanzadeh, Yusof, & Shameli, 2015e). For accurately running of NN model, data set of 10 samples were trained for learning the optimum network model. For indentify the model structure and accurate training, 2 sample data set was validated. It also stops over learning of model in training function. To evaluate the performance and predictive relationship, 2 sample of data sets was tested (Thapliyal et al., 2018). For suitable run the ANN model, forwarding multilayer NN training function with back propagation algorithm was used containing neurons in a input layer, a output layer and in a hidden layers (Thapliyal et al., 2018)(Shabanzadeh et al., 2015c). This algorithm minimize the error between experimental and predicted results by adjusting the relative weights and biases in the input and hidden layers (Thapliyal et al., 2018). The damped least-squares (DLSs) or Levenberg-Marquardt (LMA) algorithm is one of the suitable backpropagation technique applied in this study because of its quick solving capability of non-linear function (Shabanzadeh et al., 2015c)(Rostamizadeh & Rizi, 2012). The MSE with DLSs algorithm was found to be the best model.

In this current investigation, the optimal NN design was presented with prepared 14 sample data sets of  $\text{AgNO}_3$  molar concentration, %w/w of starch, gram of bentonite and Gallic acid molar concentration. The neural network running accurately using feedforward network of input layer containing 4 neurone, hidden layer contianing 10 neurones and a output layer containing 1 neuron (Thapliyal et al., 2018). For accurate prediction of AgNPs size, hyperbolic transfer function was applied with the neurons of hidden or middle layers and a linear transfer function was applied at response layer with determining their relative weight and bias values. The best fiitness of NN model was measured by calculating the training and prediction set's minimum value of the MSE. In this tool, Error goal was fixed at 0.0001 and Mu was set at 0.01 in MATLAB software R2013a version (Thapliyal et al., 2018).

By comparing all parametrs, the 4-10-1 artificial NN model containing 4 neurons in the input layer, 10 neurons in the hidden layer and 1 node in output layer with determining their relative weights and bias values measured as the best accurate fitness technique as presented in Table 6.3.

Table 6.3 *The Parameters (Connection Weight and Biases) Values for the Completed Artificial NN Technique*

<b>W<sub>1</sub></b>	<b>Input (AgNO<sub>3</sub>) 1</b>	<b>Input (Starch) 2</b>	<b>Input (Bentonite) 3</b>	<b>Input (GA) 4</b>	<b>Output (AgNPs size) 1 (W<sub>2</sub>)</b>	<b>Bias 1 (b<sub>1</sub>)</b>
<b>Node 1</b>	1.8976	-0.1242	-0.4636	1.3778	0.5291	-2.3074
<b>Node 2</b>	-1.6534	-0.1382	0.9724	-1.5202	-0.1411	1.9260
<b>Node 3</b>	1.3060	1.2060	1.3530	-0.8230	-0.2620	-1.3330
<b>Node 4</b>	-0.9216	0.7879	1.78217	0.1714	0.3389	1.05738
<b>Node 5</b>	1.3805	-1.8131	0.0888	1.0186	0.3487	-0.2741
<b>Node 6</b>	2.1674	0.6786	0.3975	-0.5637	0.0964	0.27419
<b>Node 7</b>	-1.7625	0.3435	1.3230	-1.1348	-0.6856	-0.8395
<b>Node 8</b>	0.63841	1.5851	-1.8879	-0.5614	-0.9422	1.3312
<b>Node 9</b>	-0.5128	2.2177	-0.7624	-0.6893	-0.6318	-1.9249
<b>Node 10</b>	-1.7616	-0.8808	-1.1345	-1.8225	0.2724	-2.0226
<b>Bias 2 (b<sub>2</sub>)</b>	-	-	-	-	-	0.2084

Where W<sub>1</sub> presents the weight and b<sub>1</sub> presents the bias of middle of hidden layer. W<sub>2</sub> expressed as the weight of response layer and b<sub>2</sub> expressed as the bias of response layers. Relationship between input and output has shown in Equation 6.1, where I<sub>1</sub>, I<sub>2</sub>, I<sub>3</sub>, and I<sub>4</sub> represent the input variables:

$$ANN = \text{purlin} (W_2 \times \text{transig}(W_1 \times [I_1; I_2; I_3; I_4] + b_1) + b_2) \quad \text{Equation 6.1}$$

In Equation 6.1, it is defined that well-fitting of NN model was achieved with very close relations between the experimental and the desired response values (Thapliyal et al., 2018).

### 3.1.1 Statistical analysis

Statistical performance of optimized model is an essential factor for determining the error of regression fitting. For analysis, R<sup>2</sup> and MSE parameters are measured (Shabanzadeh et al., 2015e) of all sample data sets and depicted in Table 6.4.

Table 6.4 *The Performance Assessing of NN Model on Data Sets*

Data	$R^2$	Mean square error
Training samples	0.9999	0.0010
Validation samples	1.000	0.0322
Test samples	1.000	0.0330

The training set having the  $R^2$  value is 0.9999. It determines that 99% of total difference in the data explained and model is well fitted.

Figure 6.6 describes the comparison of NN model predicted response value with experimental factors of all data sets with the help of line scattering plot. It gives the confirmation about fitness of the applied model (Thapliyal et al., 2018).

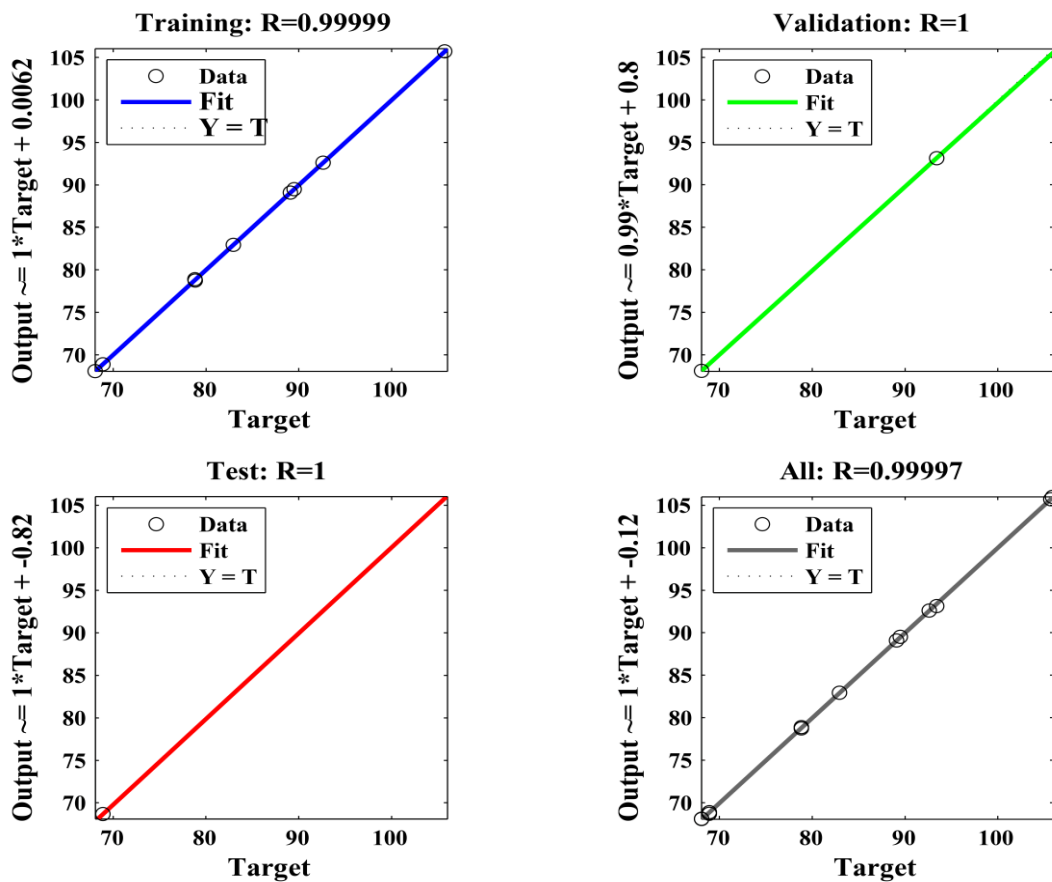


Figure 6.6. The line scatter plots of all predicted versus actual values for all train, validation and test data sets of ANN model.

Figure 6.7 represents the MSE plot of all sample data sets using 9 epochs (repetition), and the best results of validation data set is found to be 0.0323 at 4<sup>th</sup> epoch.

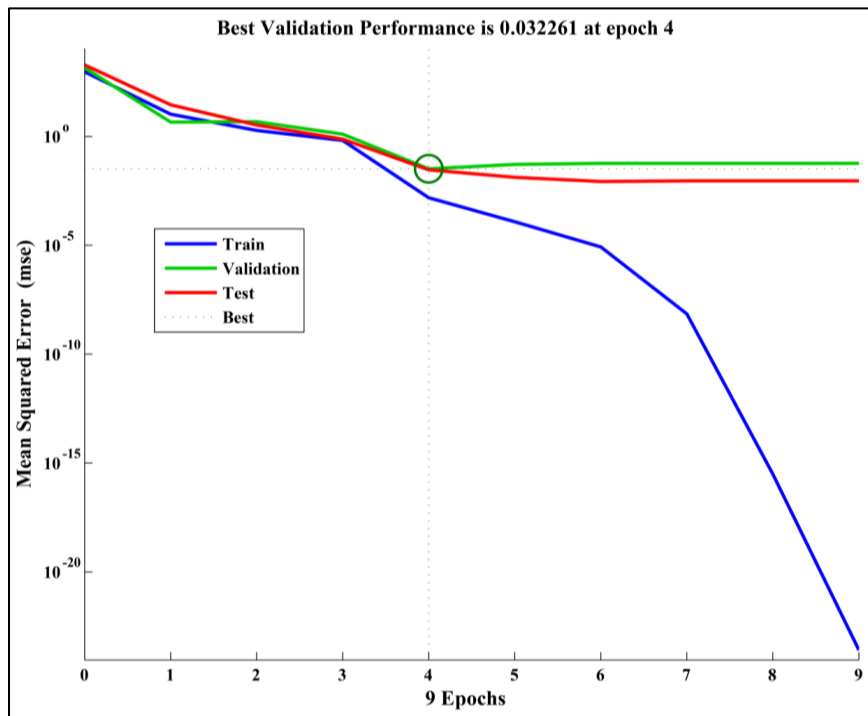


Figure 6.7. Graphical representation of mean square error values of all sample data sets.

### 3.1.2 Validation of ANN model

The optimized condition for the AgNPs synthesis in bio-nanocomposites using ANN model were depicted in Table 6.5 along with desired and actual results.

Table 6.5 *Optimized Values of Formulation and Response Variables for AgNPs Synthesis in BNCs*

Optimized parameters						% Error
AgNO <sub>3</sub> concentration in molar	(%w/w ) of Starch	Amount of Bentonite in gram	GA concentration in molar	AgNPs actual size in nm	AgNPs predicted size in nm	%Residual error
0.001	0.0005	0.003	0.004	68.060	68.061	0.002%

These results proved the model validation and the actual response value of AgNPs size was found to be very near to the Artificial NN predicted response value. It showed the

0.002% residual error (less than 1% in relative deviation), indicates that the applied ANN model can be used to properly explain the relationship between the formulation and response factors.

### 3.1.3 Model fitting analysis

Due to solving multiple regression problems, multiple linear regression (MLR) mathematical models are used to explain the relationship of explanatory independent variables with the dependent response variables (Thapliyal et al., 2018)(Shabanzadeh, Senu, Shameli, & Tabar, 2013b). It can be expressed as the following equation (Thapliyal et al., 2018):

$$Z = x + x_1 i_1 + \dots + x_n i_n \quad \text{Equation 6.2}$$

where  $Z$  expressed as the predicted response factor,  $x$  defines the regression coefficients and  $i$  expressed as the input factors and its value can be = 0,1,2,3....n (Thapliyal et al., 2018). It also describes the relationship between variables using 2-D and 3-D surface graphs.

Figure 6.8(a–d) describes the effects of each experimental factors to response (size of AgNPs) values using 2-D line graphs based on MLR model analysis. From this, it is analyzed that synergistic effect was produced in AgNPs size with increased  $\text{AgNO}_3$  concentration, starch amount, GA concentration and the Bentonite amount (Thapliyal et al., 2018).

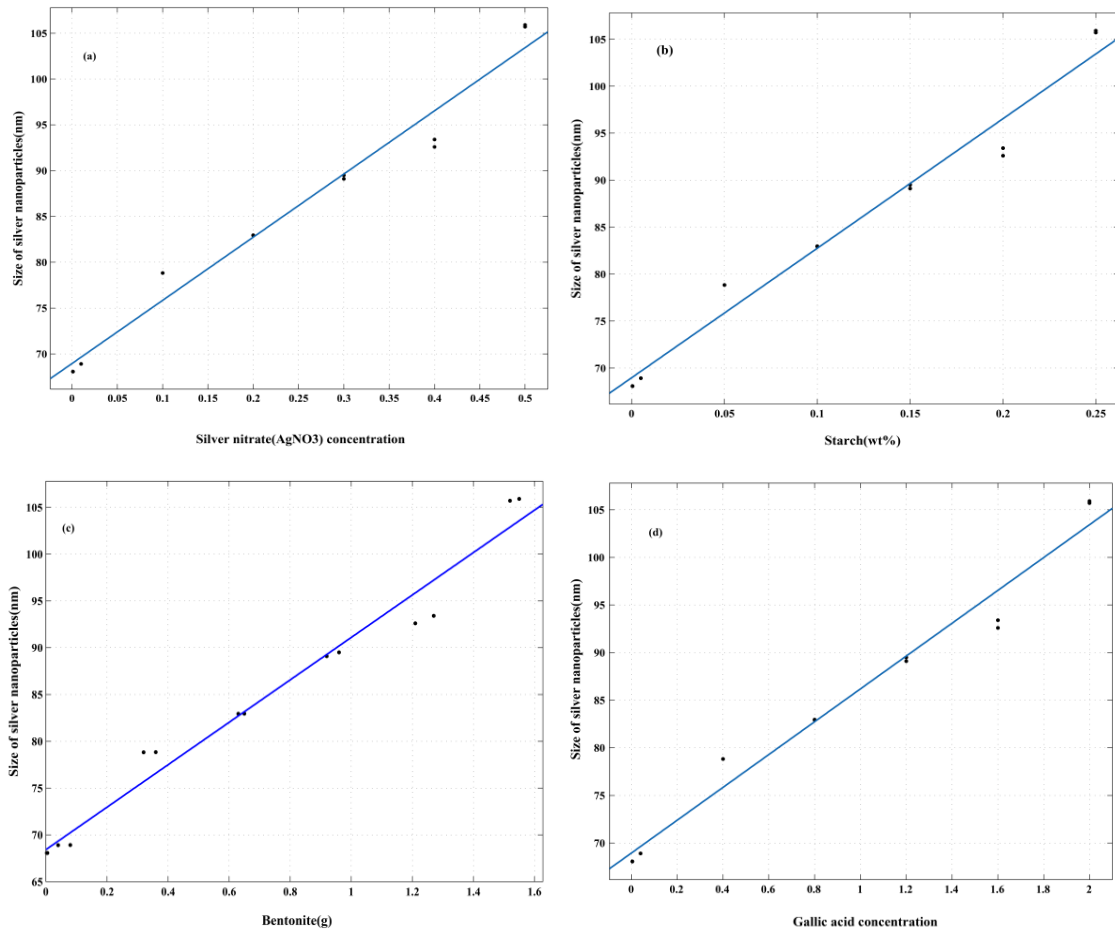


*Figure 6.8.* Two-dimensional plots (2D) effect of formulation variables (a)  $\text{AgNO}_3$  concentration (M), (b) Starch wt.%, (c) Bentonite (g) and (d) GA concentration (M) on the response variables (AgNPs size).

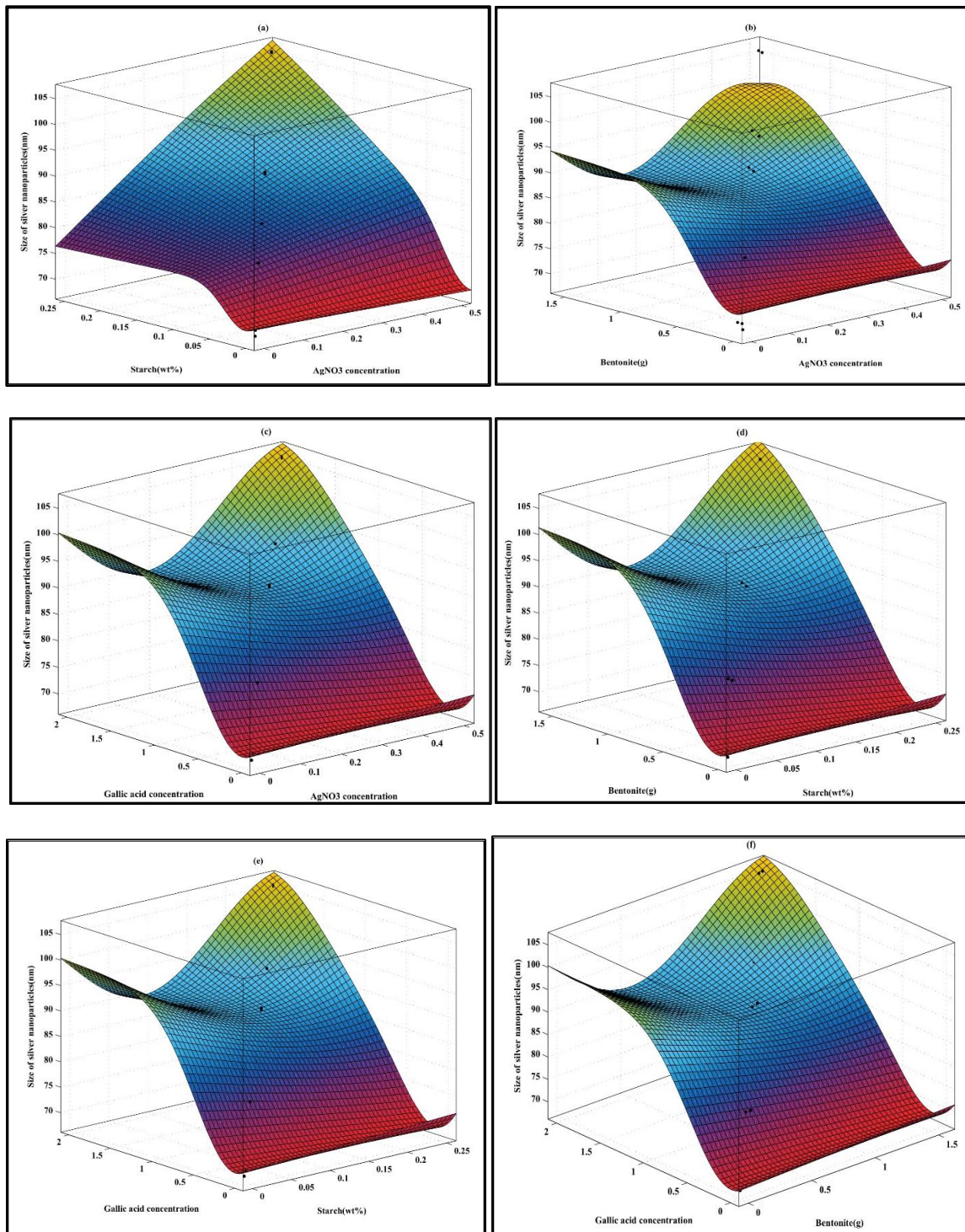


*Figure 6.9.* Three-dimensional (3D) surface plots of formulation variables (a) AgNO<sub>3</sub> conc. (M) versus Starch wt. %, (b) AgNO<sub>3</sub> conc. (M) versus Bentonite (g), (c) AgNO<sub>3</sub> versus GA conc. (M), (e) Starch wt. % versus GA conc. (M) and (f) Bentonite (g) versus GA conc. (M) with the response variables (AgNPs size).

Figure 6.9(a–f) describes the relationship of the 4 input variables with the response variables of NPs size. Figure 6.9(a) explains the effects of  $\text{AgNO}_3$  con. and starch polymer on the NPs size. The black dots in light or dark grey region can explain that conc. of  $\text{AgNO}_3$  exhibits the prominent effects on the size of nanoparticles in comparison to the starch %. It is confirmed that NPs size is effectively determined by the  $\text{AgNO}_3$  concentration (Thapliyal et al., 2018). This graph determines that: small sized silver NPs was obtained in the experimental condition,  $1 \times 10^{-3}$  M concentration of  $\text{AgNO}_3$  and 0.0005 g of Starch amount. The largest size of silver NPs was obtained in  $5 \times 10^{-1}$  M concentration of  $\text{AgNO}_3$  and 0.25 g of Starch amount. Figure 6.9(b) represents the effect on the NPs size of gram amount of Bentonite and the  $\text{AgNO}_3$  conc. The black dots in dark and light grey region explains positive effect exhibited on NPs size from increasing gram amount of Bentonite and  $\text{AgNO}_3$  conc. (Thapliyal et al., 2018). The small sized silver NPs was obtained in the experimental condition,  $1 \times 10^{-3}$  M concentration of  $\text{AgNO}_3$  and 0.003 g of Bentonite amount. The largest size of silver NPs was obtained in  $5 \times 10^{-1}$  M concentration of  $\text{AgNO}_3$  and 1.55 g of Bentonite amount. In Figure 6.9(c) the black dots placed inside the dark and light grey region indicates that both GA and  $\text{AgNO}_3$  conc. determines NPs size equally. It is concluded that small sized silver NPs was obtained in the experimental condition,  $1 \times 10^{-3}$  M concentration of  $\text{AgNO}_3$  and  $4 \times 10^{-3}$  M concentration of GA. Also, the largest size of silver NPs was obtained in  $5 \times 10^{-1}$  M concentration of  $\text{AgNO}_3$  and  $20 \times 10^{-1}$  M concentration of GA. Figure 6.9(d) defines that polymer starch is a more effective than clay of Bentonite for NPs size. Therefore, small sized silver NPs was obtained in 0.0005 g of Starch amount and 0.003 g of Bentonite amount and also, the largest size of silver NPs was obtained in 0.25 g of Starch amount and 1.55 g of Bentonite amount. Figure 6.9(e) describes that GA drug is more effective for effecting NPs size in compared to the polymer starch (Thapliyal et al., 2018). Therefore, small sized silver NPs was obtained in 0.0005 g of Starch amount and  $4 \times 10^{-3}$  M concentration of GA and also, the largest size of silver NPs was obtained in 0.25 g of Starch amount and  $20 \times 10^{-1}$  M concentration of GA. The effect of GA drug conc. and the gram amount of bentonite were explained in Figure 6.9(f). It shows that the black dots in the dark and light grey region exhibits similar effect of both of GA drug conc. and gram amount of bentonite. It is concluded that small sized silver NPs was obtained in  $4 \times 10^{-3}$  M concentration of GA and 0.003 g of Bentonite amount also, the

largest size of silver NPs was obtained in  $20 \times 10^{-1}$  M concentration of GA and 1.55 g of Bentonite amount. Figure 6.9(a–f) explains that the silver precursor  $\text{AgNO}_3$  and reducing agent GA conc. exhibits large effect on the NPs size in compared to the other variables. These two variables make the significant effect in the NPs size, while similar effects exhibits by both other excipients like starch polymer and bentonite clay (Thapliyal et al., 2018). In conclusion, the sizes of AgNPs increased with the enhanced silver precursor ( $\text{AgNO}_3$  concentration), polymer starch %, the gram amount of Bentonite and GA concentration.

### 3.2 Characterization techniques of optimized AgNPs in BNCs formulation

#### 3.2.1 UV-visible absorption spectral analysis

The synthesis of AgNPs in the BNCs was recorded by the color changing ability of solution from light brown to dark brown. The absorption maxima were recorded at a wavelength of 200–800 nm. Figure 6.10 presents the UV-Vis spectra of GA, Ag/bentonite/starch composites and AgNPs respectively. The UV spectrum identify an absorption peak at 412 nm, which confirmed the formation of homogenously dispersed AgNPs in BNCs (Thapliyal & Chandra, 2018). Figure 6.10 indicates that the binding of GA with Ag resulted in a red shift of the absorption band of AgNPs at a higher wavelength of 412 nm.

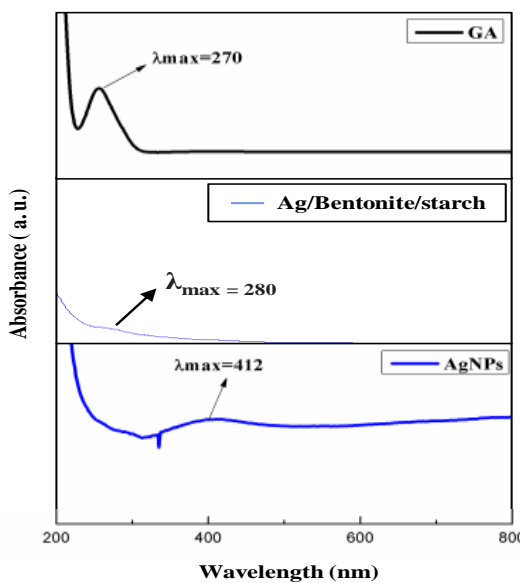


*Figure 6.10.* UV-vis absorption spectra and visible observation of GA, Ag/bentonite/starch composite and AgNPs synthesized in BNCs.

### 3.2.2 Size and dispersity index (PDI) of AgNPs

The AgNPs particle size was found in a scale of  $68\text{-}106\pm0.25$  nm (mean $\pm$  SD,  $n=3$ ). The PDI of nanoparticles was found between 0.2-0.8, which confirms the monotonous particles distribution. The NPs size of optimized formulation was found  $68.06\pm0.25$  with PDI  $0.03\pm0.12$  which confirmed the uniform distribution of particles (Figure 6.11).

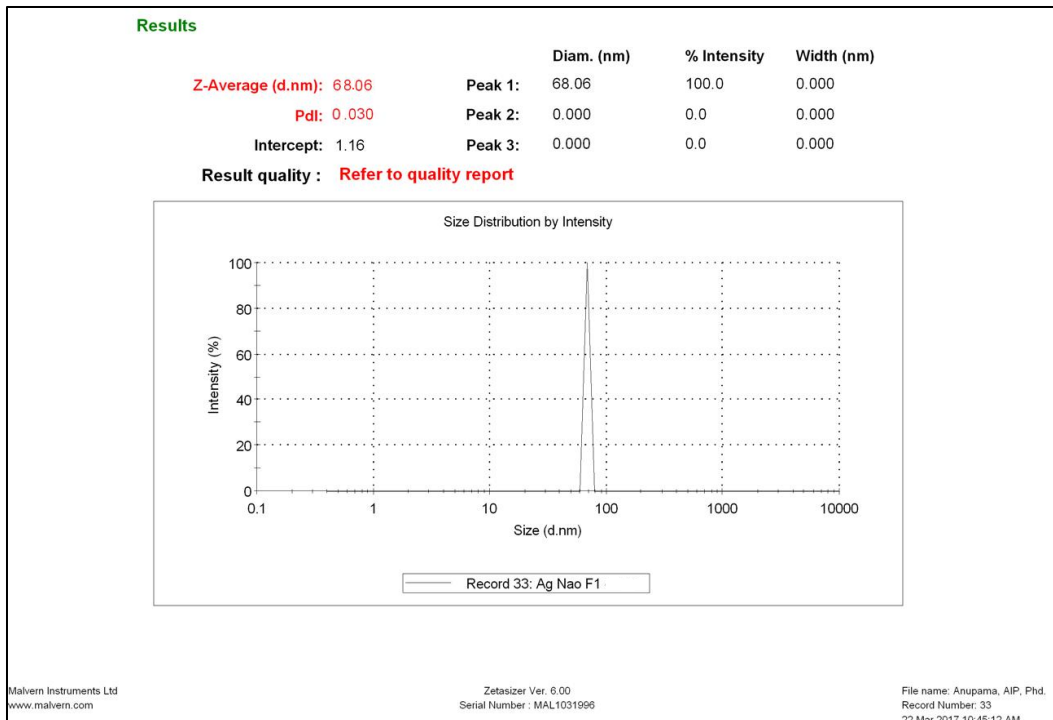


Figure 6.11. DLS report of optimized AgNPs.

### 3.2.3 Scanning electron microscopy (SEM) and energy dispersive x-ray analysis (EDXA)

SEM determined the morphological surface, shape, and size of silver nanoparticles. Figure 6.12 shows the different magnification of SEM images of synthesized AgNPs in BNCs. It is determined that spherical shaped AgNPs was formed less than 100 nm.

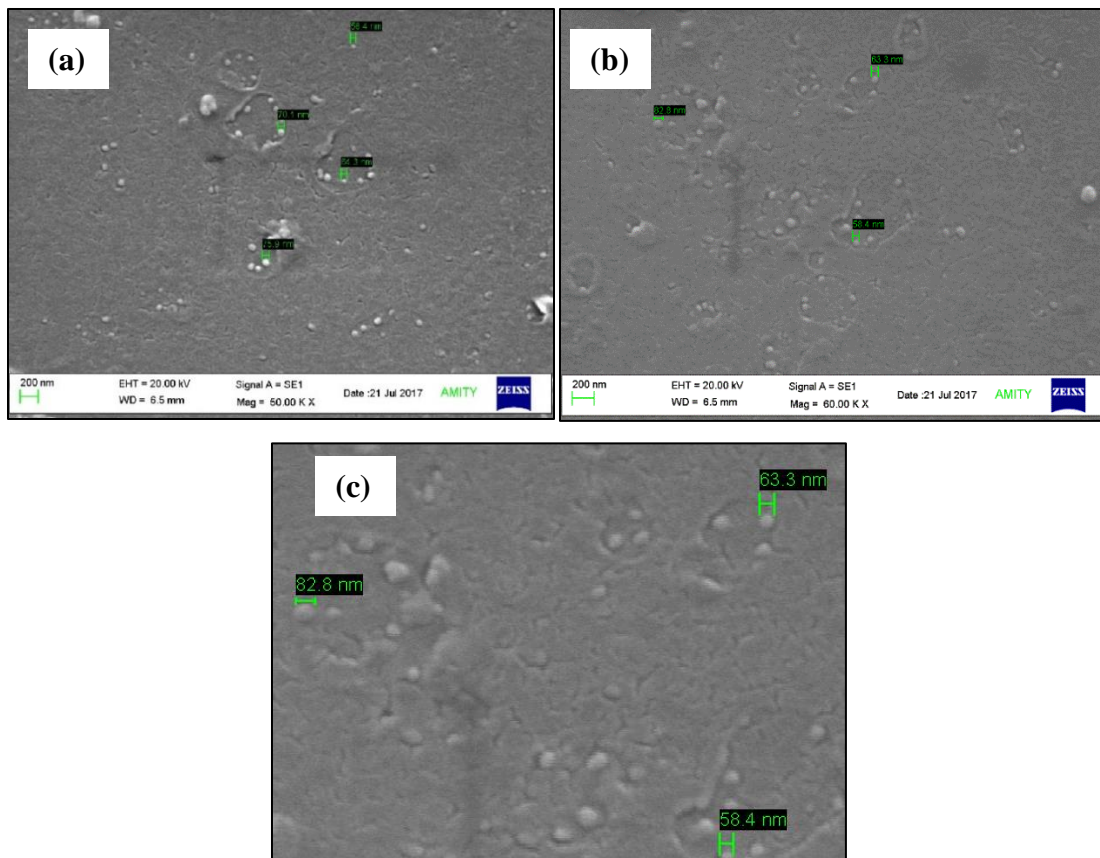


Figure 6.12. Scanning electron microscopic images of synthesized AgNPs in BNCs at (a-b) lower magnification and at (c) higher magnification.

The elemental analysis of AgNPs is carried out by using EDXA analysis is presented in Figure 6.13. EDXA spectrum exhibits the strong peak at 3.12 keV is matching to the binding energies of Ag (Kaviya, Santhanakshmi, Viswanathan, Muthumary, & Srinivasan, 2011) and confirming the formation of the synthesized AgNPs in BNCs. It is also confirmed the presence of elemental compounds with no other impurity peak.

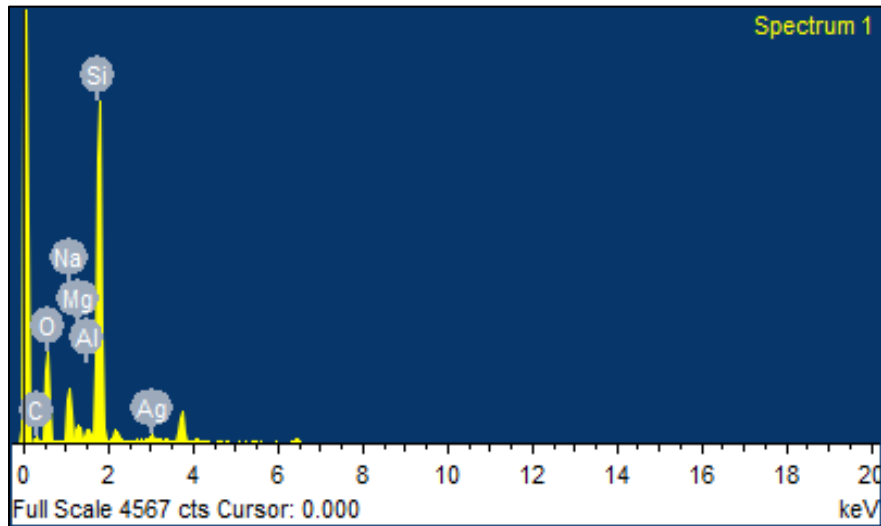


Figure 6.13. EDXA spectrum of synthesized AgNPs in BNCs.

### 3.2.4 X-ray diffraction (XRD) study

The structural behaviour of the AgNPs was analyzed using the XRD technique. Figure 6.14 describes the XRD graph of dried optimized AgNPs formulation. The intensity was recorded at 20 to 60°. The XRD graph of AgNPs confirmed its face-centred isometric (cF) crystalline structure. The crystallographic plane located of 111 at 2θ of 38.26° and 200 at 2θ of 44.29° indicates the silver NPs are crystalline in nature (Thapliyal et al., 2018) which is in agreement with the standard powder diffraction card of Joint committee on Powder Diffraction Standard (JCPDS) of Ag file No. 04-0783. It concludes that the crystalline nature with same diffraction pattern was observed in synthesized AgNPs in BNCs.

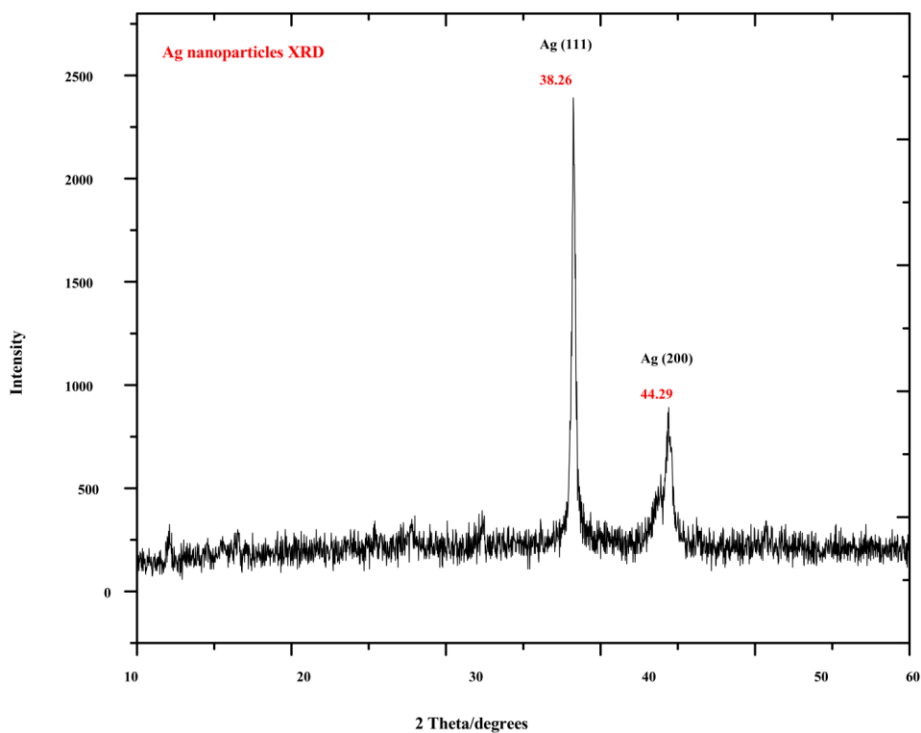


Figure 6.14. XRD graph of synthesized AgNPs in BNCs.

### 3.2.5 Zeta potential determination (ZP)

The ZP determines the colloidal stability of particles. It is an essential parameter for measuring the particles surface charge and it predicts the storage stability of colloidal particles. Figure 6.15 indicates the zeta potential measurement of optimized AgNPs was found  $-32\text{mV}$  with conductivity  $4.89 \text{ mS/cm}$  (Thapliyal & Chandra, 2018). This large negative value indicates the good colloidal nature due to negative-negative repulsion, monotonous dispersity of AgNPs and great stability with longer storage time.

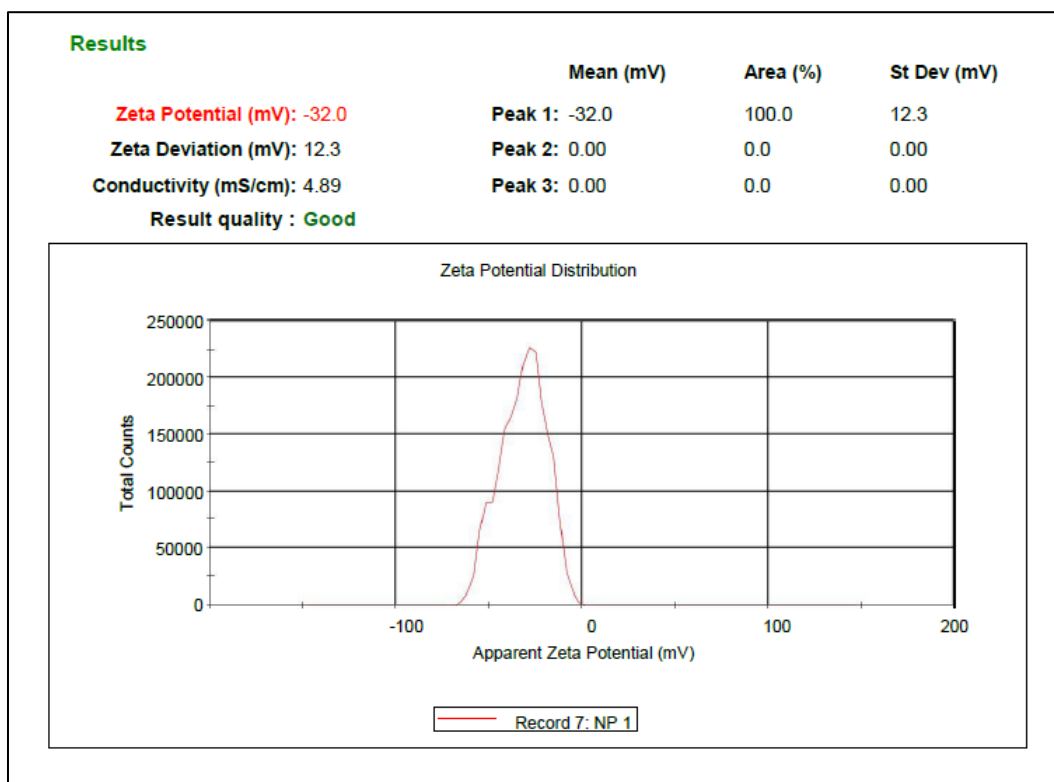


Figure 6.15. Diagrammatic representation of zeta potential of synthesized AgNPs in BNCs.

## 3.3 Evaluation of optimized AgNPs in BNCs formulation

### 3.3.1 Inductively coupled plasma mass spectrometry (ICP-MS) study

ICP-MS analysis is a method used for identifying the concentration of silver (Ag) in the formulations in time dependent manner. Figure 6.16 presents the ICP-MS graph of silver. It was observed that  $0.72 \pm 0.02 \text{ ppm}$  of Ag was found in the nanoparticles, accounting for 64.8% of the total amount of Ag released from nanoparticles within 24h.

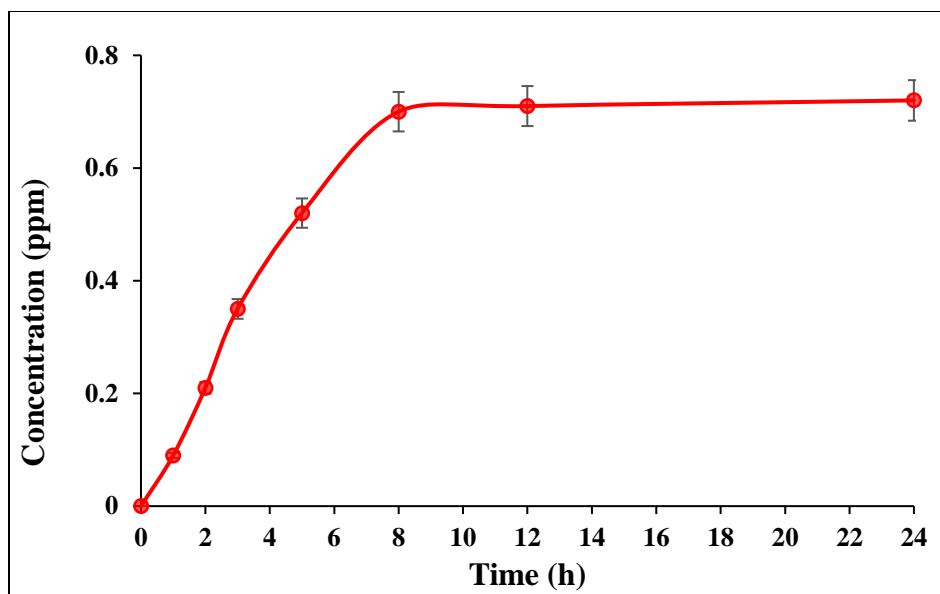


Figure 6.16. ICP-MS graph of silver release from AgNPs. Data was presented as mean $\pm$ SD (n=3)

### 3.3.2 Entrapment efficiency (EE) and loading efficiency (LE) of GA

The %drug loading and %EE in optimized AgNPs were found to be 83.5 and  $80.23\pm0.25\%$  (mean $\pm$  SD, n=3) respectively. It is concluded that GA was uniformly distributed in the nanoparticles and drug loss was minimum during the synthesis of the silver NPs (Thapliyal & Chandra, 2018).

### 3.3.3 *In vitro* drug release analysis

Figure 6.17 presents the *in vitro* drug release study of the optimized AgNPs at pH 5 and pH 7.4. It is observed that  $92\pm0.02\%$  drug release was achieved at cancer cells pH 5 in comparison to the  $68\pm0.05\%$  at pH 7.4 over the period of 24 h. Optimized AgNPs showed a burst release of the drug at the initial stage and then exhibited an extended release over the 24 h., The slowest drug release was observed at systematic pH of 7.4, and the greater release was recorded in pH 5, which is the pH of cancer cells. It is concluded that the AgNPs can be used as an effective oral drug delivery system for targeting cancer because of its pH-sensitive properties. AgNPs in BNCs system exhibit the active drug release in the acidic environment of cancer cells which increases therapeutic concentration of drug to cancer cells compared to healthy cells (Thapliyal & Chandra, 2018).

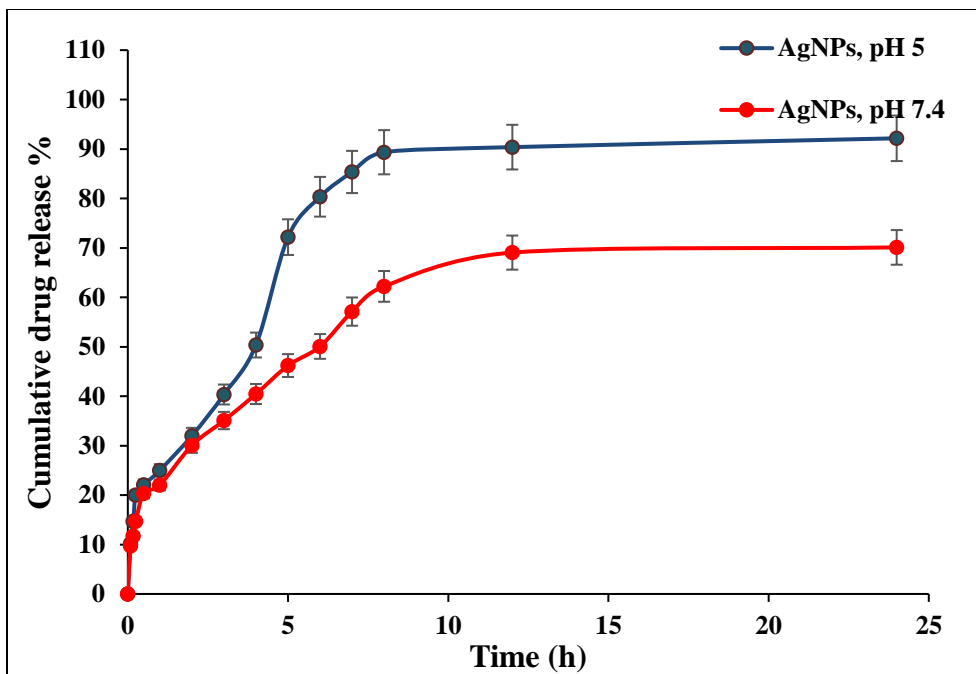
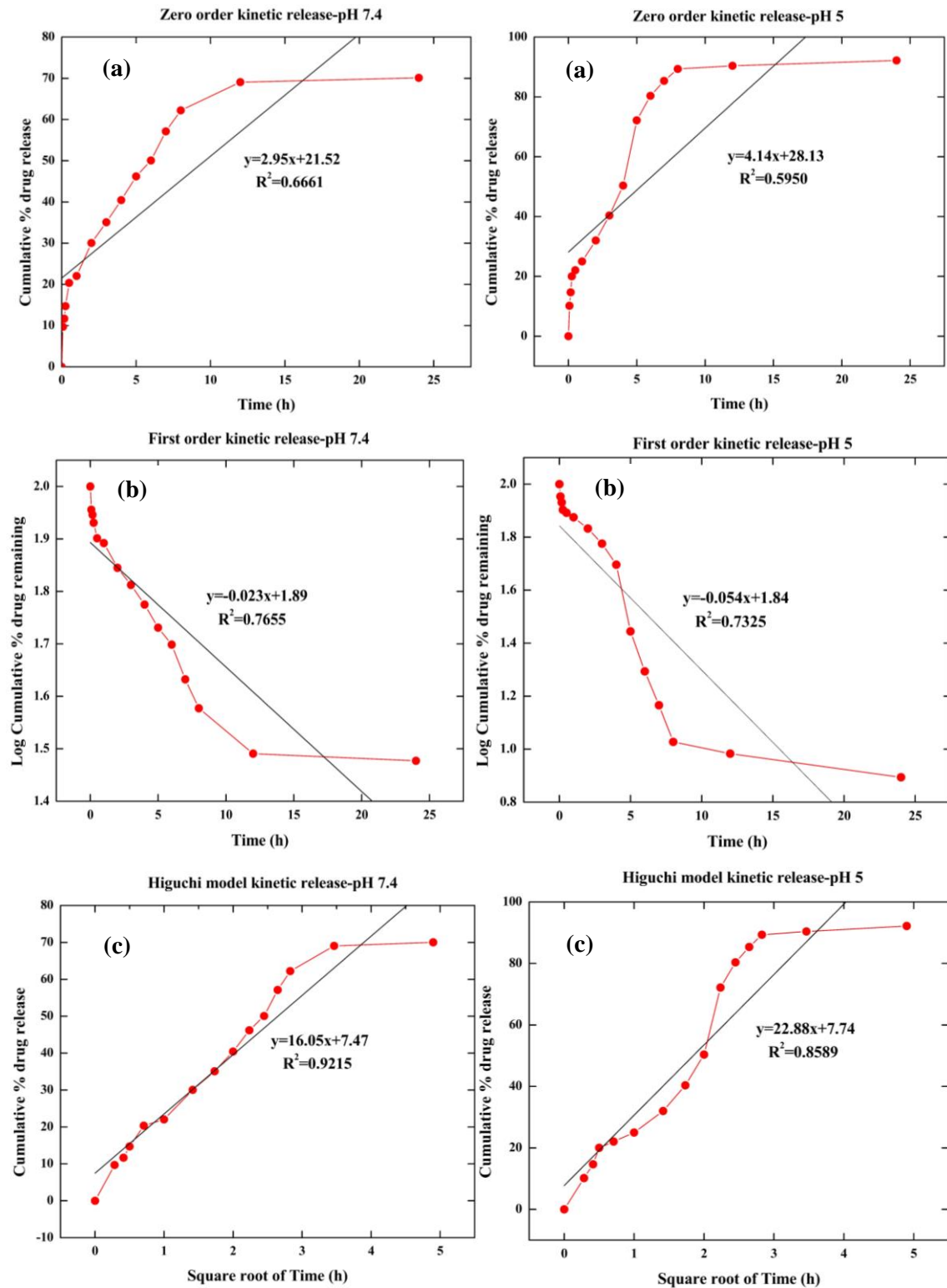


Figure 6.17. *In-vitro* drug release from optimized AgNPs in BNCs in pH 5 and pH 7.4. Data was shown as mean $\pm$ SD (n=3)

### 3.3.4 Release kinetics

To investigate the GA release kinetic mechanisms from AgNPs loaded ME, the result of *in vitro* analysis of data was placed into five different kinetic tools such as (i) Zero model (time/cumulative % drug released), (ii) Ist order (time/log of cumulative% drug retained), (iii) Higuchi model ( $\sqrt{T}$  /cumulative % released), (iv) Peppas model (log of time/cumulative % drug released) and (v) Hixon ( $W_0-W_t$  versus time) as depicted in Figure 6.18. Based on the kinetic analysis of higher regression,  $R^2$  value (Table 6.6) it was determined that the GA release from AgNPs at pH 7.4 and pH 5 followed the Korsmeyer-peppas model and it was best predominant release mechanism fitted followed by Higuchi model. The ‘n’ values of 1.3 and 1.4 of the Korsmeyer–peppas equation suggested that the drug follows the non-fickian diffusion of drug release behavior which is a super case II release kinetics (Thapliyal & Chandra, 2018)(Kuksal, Tiwary, Jain, & Jain, 2006). These results indicated that the drug followed diffusion mechanism from the polymer matrix and may be controlled by polymer swelling or erosion, or by these mechanism altogether (Emara, Taha, & Mursi, n.d.).



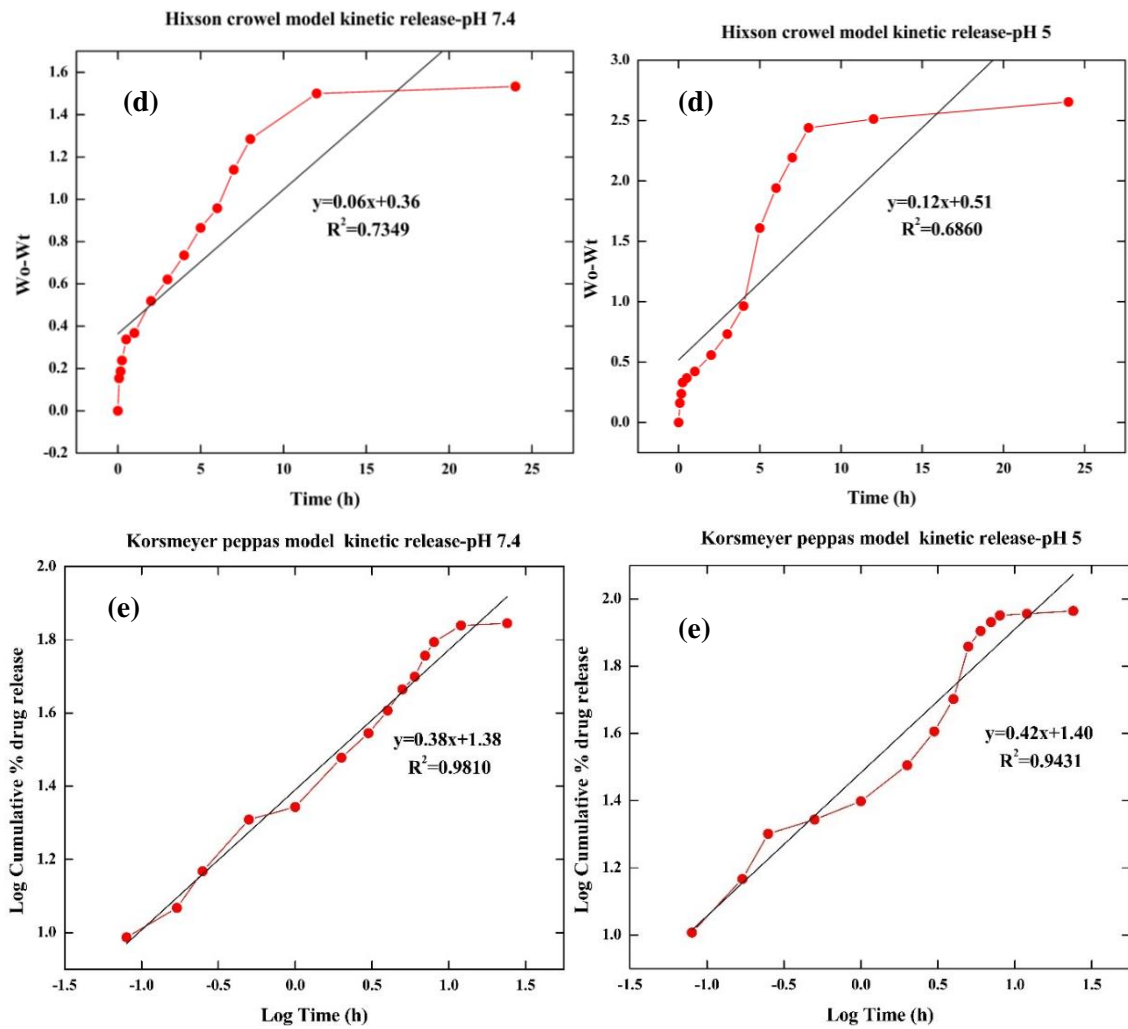


Figure 6.18. Graphical representation of drug release kinetics mechanism of synthesized AgNPs in BNCs at (a-e) pH 7.4 and (a-e) pH 5 for Zero, Ist order, Higuchi, Korsmeyer-peppas and Hixson model.

Table 6.6 *Release Kinetic Models and Their Release Parameters*

Kinetic model	Zero-order reaction model	Ist order reaction model	Higuchi reaction model	Korsmeyer-Peppas reaction model	Hixon crowel reaction kinetic model	
	<b>k</b>	<b>R<sup>2</sup></b>	<b>k</b>	<b>R<sup>2</sup></b>	<b>n</b>	<b>R<sup>2</sup></b>
pH 7.4	2.95	0.6661	0.023	0.7655	16.05	0.9215
pH 5	4.14	0.5950	0.054	0.7325	22.88	0.8589

## 4. Synthesis of AgNPs loaded Microemulsion

### 4.1 Screening of microemulsion region

#### 4.1.1 Pseudo-ternary plot

For determining the composition of *w/o* microemulsion formation region, the ternary phase diagram was constructed. Figure 6.19(a and b) indicates the pointed areas for the synthesis of  $\text{AgNO}_3$  and GA microemulsion in the ternary phase diagram. Oil content ranging from 45-60% (*w/w*), Surfactant content ranging from 20-35% (*w/w*) and the silver and reducing precursor in the range of 8-22% (*w/w*) was chosen using phase diagram for the synthesis of the microemulsion.

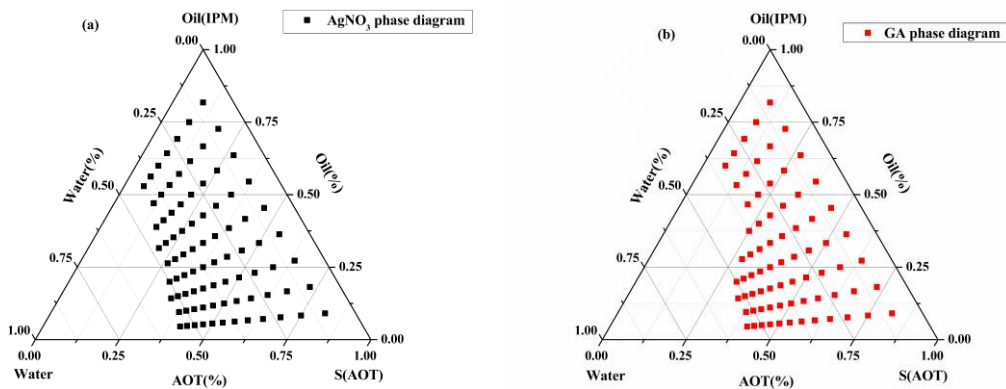


Figure 6.19. Pseudo-ternary phase diagram for water-in-oil microemulsion systems containing (a) silver precursor ( $\text{AgNO}_3$ ) and (b) reducing agent (GA).

### 4.2 D-Optimal mixture experimental technique

The mixture design of D-optimal with 3-factor with 4-response was used for optimization and analysis of the bonding between the formulation and response variables. The mixture components cannot range independently since their sum has to be equal to 100% (Samson, Basri, Fard Masoumi, Abedi Karjiban, & Abdul Malek, 2016b)(Nahata & Saini, 2008). Table 6.7 lists the limitations of the formulation variables. Table 6.8 presents the 12 experimental run matrixes generated using software application Design-Expert technique 10.0.0 version which consisting 12 different mixtures of oil, aqueous solution, and surfactant and analyzing their relationship with output variables.

Table 6.7 *Constraints of Mixture Components Proportions*

Design Constraints			
Mixture Coding:	<b>Actual</b>		
<b>Low limit (<math>L_i</math>) <math>\leq</math></b>	<b>Constraint(Independent variables, <math>X_i</math>) <math>\leq</math></b>		
45.000 $\leq$	$X_1$ :Oil (IPM) $\leq$		60.000
20.000 $\leq$	$X_2$ :Surfactant (AOT) $\leq$		35.000
8.000 $\leq$	$X_3$ :Aqueous solution $\leq$		22.000
	$X_1+X_2+X_3$	=	100.000

Table 6.8 *The 12 sets of An Experimental Run for Optimizing Water-in-Oil Microemulsion Obtained by D-optimal Mixture Design and Their Response Values*

	Component X1	Component X2	Component X3	Response 1	Response 2	Response 3	Response 4
Run	A: Oil (IPM) %	B: Surfactant (AOT) %	C: Aqueous solution %	Particle size(nm)	Viscosity (cps)	pH	%Drug Release
1	58.00	20.00	22.00	25.00	23.40	7.45	70.00
2	60.00	25.22	14.78	37.00	31.60	5.83	74.60
3	49.86	32.95	17.19	34.30	47.00	5.87	80.81
4	55.28	24.76	19.99	12.80	56.80	5.92	81.28
5	52.59	35.00	12.41	95.90	57.00	5.95	84.00
6	47.26	30.73	22.00	71.00	50.90	5.92	81.20
7	45.00	35.00	20.00	135.40	63.00	6.86	70.00
8	60.00	21.88	18.12	23.00	22.00	6.80	68.21
9	57.25	30.44	12.31	41.77	70.81	5.23	85.00
10	54.35	29.30	16.35	3.39	67.00	5.37	85.00
11	60.00	32.00	8.00	160.70	78.00	5.17	85.42
12	50.71	27.29	22.00	25.71	40.01	5.50	85.51

#### 4.2.1 Fitting the model

A special quartic and quadratic model with minimum predicted residual sum of square (PRESS) statistic was fitted to the all four experimental responses using D-optimal mixture software. A minimum value of PRESS statistic is usually considered as the most predictive model for the given set of data (Barot, Parejiya, Patel, Gohel, & Shelat, 2012b). Lambda value of 1 was required to provide the best fit and the improvement of the model. Table 6.9 shows the values of the statistical parameter generated by the Design Expert

technique of all four response variables. The adjusted and predicted  $R^2$  values of four responses does not show the difference greater than 0.01; it means the model could not explain only less than 0.01% of the total variance (Nahata & Saini, 2008). It concludes a close fit in the middle of the actual and model desired values and also confirmed the suitability of selected models.

Table 6.9 *Model Summary Statistics of Response Variables*

Response variable	Types of model	*F-statistic value	* Df	Prob (p value >F)	R-Squared	Adjusted R <sup>2</sup>	Predicted R <sup>2</sup>	PRESS
<b>Y1(Particle size)</b>	Special Quartic	55.40	3	0.0040	0.9995	0.9982	0.9843	435.89
<b>Y2(Viscosity)</b>	Special Quartic	471.9	3	0.0001	0.9999	0.9998	0.9960	15.16
<b>Y3 (pH)</b>	Quadratic	377.30	3	0.0001	0.9967	0.9939	0.9873	0.069
<b>Y4(%Drug release)</b>	Quadratic	824.70	3	0.0001	0.9983	0.9968	0.9882	5.80

\*Df: degree of freedom; F-value: Fischer function

#### 4.2.2 Analysis of variance (ANOVA)

ANOVA was used to analyze the fitness of the assumed mathematical model using the DOE (Design Expert) software. ANOVA outcomes of four responses are presented in Table 6.10. The model  $F$ -statistics value (Fischer's function) of Y1 to Y4 is 55.4, 471.9, 377.30 and 824.70 respectively imply the significances of applied model. The  $p$ -value is defined as the probability of reaching the  $F$ -statistics value (Jeirani et al., 2012b). The model  $p$ -value of Y1 to Y4 < 0.0001 confirms significances of optimized model. Table 6.11 shows that interaction coefficient terms(AB, AC, BC, AC) and quadratic coefficient terms( $A^2BC$ ,  $AB^2C$ ,  $ABC^2$ ) are significant because their  $p$ -values are < 0.05. The signal-to-noise ratio measured by adequate precision was found to be 86.042, 230.564, 58.06 and 65.48 of Y1, Y2, Y3 and Y4 respectively. Table 6.10 lists the value of PRESS, SD, mean

and coefficient of variation (C.V.) value, which are a clear indication of an accurate and well-fitted model.

Table 6.10 ANOVA Table of The Optimized Mixture Design Model

Sum of Squares															
Response	Model	Linear Mixture	AB	AC	BC	A <sup>2</sup>	B <sup>2</sup>	C <sup>2</sup>	Residuals	Cor total	Std.	Mean	C. V %	Ad. Precision	
Y1(Particle size)	2770 2.42	127 93. 95	32 88. 19	44 39. 73	27 86. 06	11 8. 48	40 5. 11	38 9. 83	13.5 1 93	277 15. 93	2. 1 2	55 .5	3. 82	86. 042	
Y2(Viscosity)	3777 .3	232 1.9 6	72. 99	39 6.9 9	22 5.6 8	30 .9 5	67 2. 39	28 .3 7	0.23	377 7.5 3	0. 2 8	50 .3 8	0. 55 4	230 .56 4	
Y3(pH)	5.45	2	3	0.0 26	0.7 6				0.01 8	5.4 7	0. 0 5 5	5. 99 92	0. 58. 006		
Y4(%Drug release)	490. 08	137 .78	32 9.4 2	12. 16	1.8 2				0.85	490 .93	0. 3 8	79 .2 5	0. 48	65. 483	
df value															
Y1-Y2	8	2	1	1	1	1	1	1							
Y3-Y4	5	2	1	1	1					11					
Mean Square															
Y1(Particle size)	346 2.8	639 6.9	32 7	44 19	27 73	11 06	40 48	38 11							
Y2(Viscosity)	472 .16	116 0.9	72. 8	39 6.9 9	22 5.6 8	30 .9 5	67 2. 39	28 .3 7							
Y3(pH )	1.0 9	1	3	0.0 26	0.7 6										
Y4(% Drug release )	98. 02	68. 89	32 9.4 2	12. 16	1.8 2										

“Table 6.10 (continued).”

Response	Model	Linear Mixtu re	AB	AC	BC	A <sup>2</sup> B C	A <sup>2</sup> B <sup>2</sup> C	AB C <sup>2</sup>	Residu als	Cor tot al	St d.	M ea n	C. V %	Ad. Pre cisi on
<i>F</i> -value														
Y1(Particle size)	769 .09	142 0.7 8	73 0.3 1	98 6.0 7	61 8.7 9	26 .3 2	89 .9 8	86 .5 8						
Y2(Viscosity)	605 7.8 4	148 95. 36	93 6.4 9	50 93. 39	28 95. 52	39 7. 15	86 26 .8	36 4. 02						
Y3(pH )	357 .47	327 .71	98 2.6 1	8.4 9	25 0.4 7									
Y4(% Drug release )	688 .33	483 .79	23 13. 46	85. 38	12. 76									
<i>p</i> -value <i>Prob</i> > <i>F</i>														
Y1(Particle size)	<0.001	<0.001	0.01	<0.001	0.01	0.43	0.25	0.26						
Y2(Viscosity)	<0.001	<0.001	<0.001	<0.001	<0.001	0.03	<0.001	0.03						
Y3(pH )	<0.001	<0.001	<0.001	<0.026	<0.008									
Y4(% Drug release )	<0.001	<0.001	<0.001	<0.001	0.011									

In Table 6.11, the positive regression coefficients indicates synergistic effects between factor and responses variables and a negative value of coefficients defines an opposite effect among the input and output variables (Samson et al., 2016b). From the analysis using Design expert, the most significant effect observed on the responses by factor C ( $\text{AgNO}_3$  and GA precursor).

Table 6.11 *Regression Coefficient Table of D-optimal Mixture Model*

Coefficient Estimate									
Response	A-Oil (IPM)	B-Surfactant (AOT)	C-Aqueous solution	AB	AC	BC	A <sup>2</sup> BC	AB <sup>2</sup> C	ABC <sup>2</sup>
Y1(Particle size)	178.50	49.90	257.82	-388.40	-516.71	-417.01	-1244.55	2227.12	-2018.00
Y2(Viscosity)	74.77	23.23	110.73	-57.87	-154.51	-118.69	-636.13	2869.25	544.42
Y3(pH)	7.17	8.50	5.42	-8.77	-0.89	-5.51			
Y4(%Drug release)	65.02	59.87	89.66	91.89	19.39	8.50			
<i>df value</i>									
Y1-Y2	1	1	1	1	1	1	1	1	
Y3-Y4	1	1	1	1	1	1			
Standard Error									
Y1(Particle size)	3.19	3.08	4.30	14.37	16.45	16.76	242.61	234.79	216.88
Y2(Viscosity)	0.42	0.41	0.57	1.89	2.17	2.21	31.92	30.89	28.53
Y3(pH)	0.072	0.071	0.099	0.28	0.31	0.35			
Y4(%Drug release)	0.49	0.48	0.68	1.91	2.10	2.38			
95% CI low									
Y1(Particle size)	168.36	40.08	244.14	-434.14	-569.08	-470.36	-2016.63	1479.91	-2708.19
Y2(Viscosity)	73.43	21.94	108.93	-63.89	-161.40	-125.71	-737.71	2770.94	453.61
Y3(pH)	7.00	8.32	5.18	-9.45	-1.65	-6.36			
Y4(%Drug release)	63.83	58.69	88.00	87.22	14.25	2.68			
95 % CI High									
Y1(Particle size)	188.64	59.71	271.51	-342.66	-464.35	-363.66	-472.46	2974.32	-1327.81

“Table 6.11 (continued).”

Response	A-Oil (IP M)	B-Surfactant (AOT)	C-Aqueous solution	AB	AC	BC	$A^2BC$	$AB^2C$	$ABC^2$
<b>Y2(Viscosity)</b>	76.10	24.52	112.53	-51.85	147.62	-111.67	-534.54	2967.56	635.23
<b>Y3(pH)</b>	7.35	8.67	5.67	-8.08	-0.14	-4.66			
<b>Y4(%Drug release)</b>	66.22	61.05	91.31	96.57	24.52	14.32			

Before prediction of optimized microemulsion formulation composition, a normal residual analysis was carried out to confirm that fitting of ANOVA parameters is met. Figure 6.20 indicates the line plot of desired versus experimental value of globule size, viscosity, pH and % Drug release. It confirms the fitting of ANOVA parameters of the selected design and gives the close fit between predicted and actual responses.

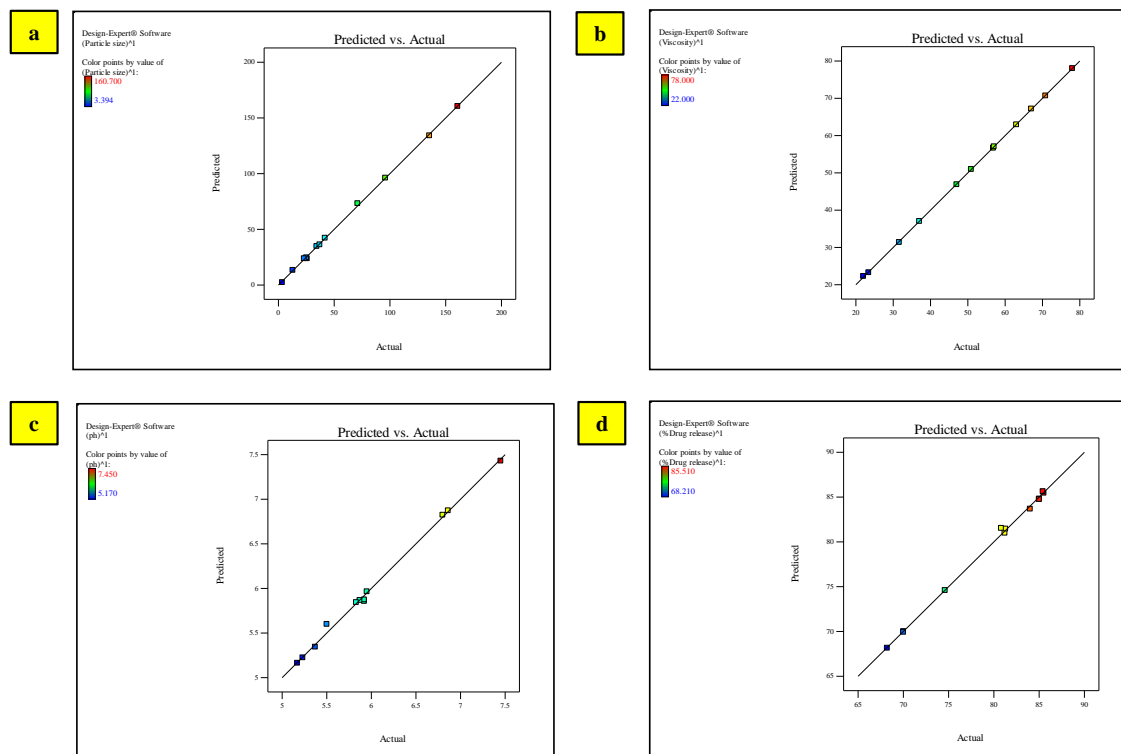


*Figure 6.20.* The line scatter graphs of model predicted versus experimental response, i.e.(a) Particle size, (b) Viscosity, (c) pH and (d) % Drug release from D-optimal mixture design.

### 4.2.3 Diagnostics

Figure 6.21 presents the normal probability plot showing the residual analysis of the model. The points lying on the straight line indicates that the fitted model were normally distributed with residuals and the model has been validated (Jeirani et al., 2012b).

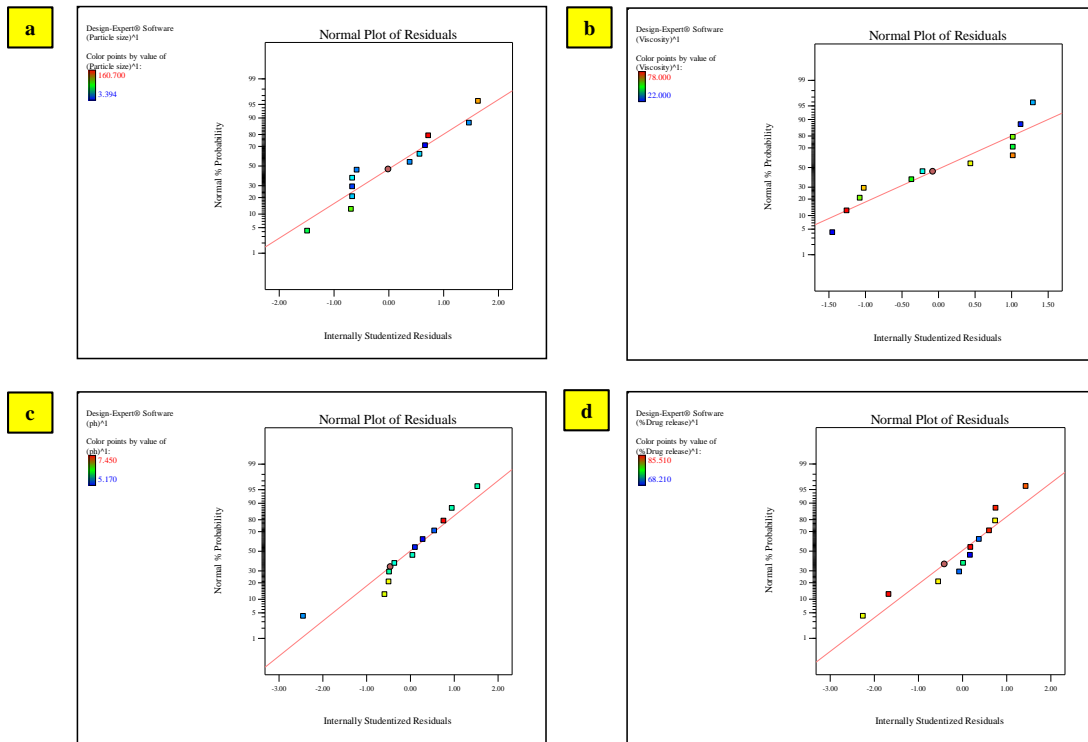


*Figure 6.21.* The normal plot of residual of (a) Particle size, (b) Viscosity, (c) pH and (d) % Drug release.

Figure 6.22 depicts the second diagnostic tool; Box-Cox Plot which confirmed the model validation. Figure 6.22(a-d) presents the Box-cox plot of four response variables. The blue line representes the value of Lambda = 1 with current trasfer and the dark green line shows the best lambda value of globular size, viscosity pH and drug release is 0.93, 1, 0.92 and 0.37 respectively obtained using Box-cox plot which is close to 1, while the red lines indicate  $p < 0.05$ . In conclusion, the model is a close fit to the actual data and meets the expectations of the ANOVA parameters.

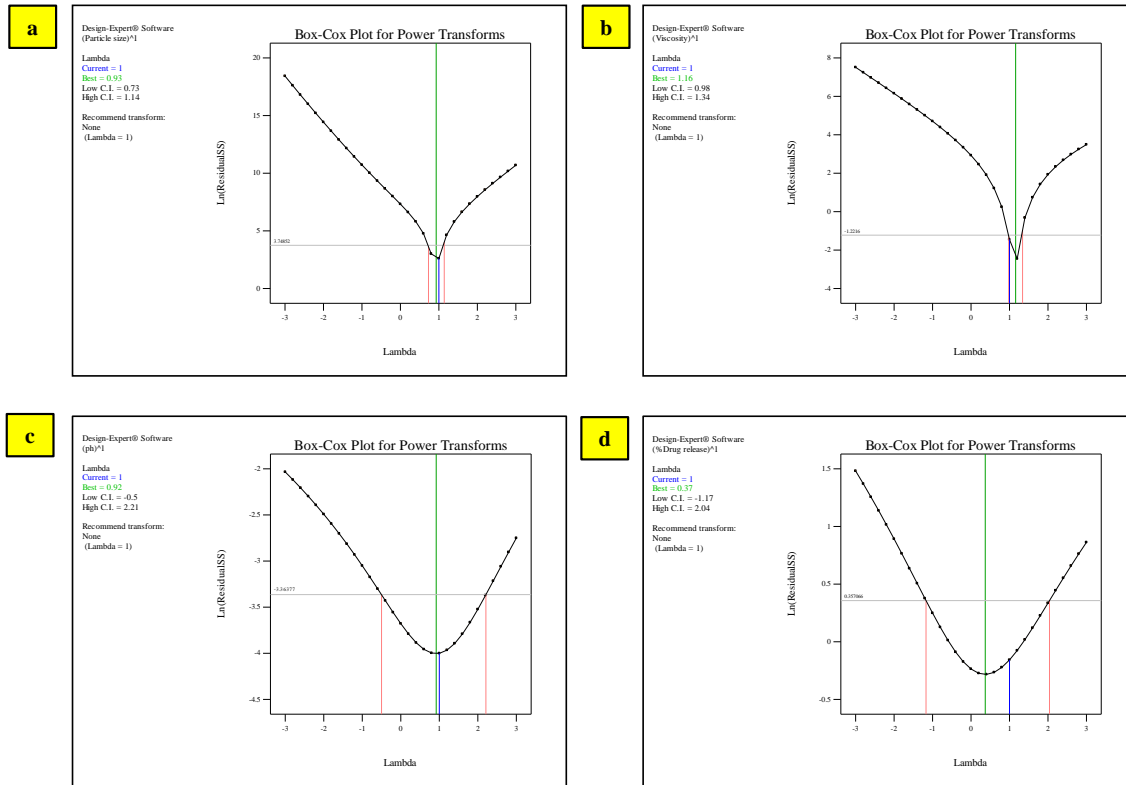
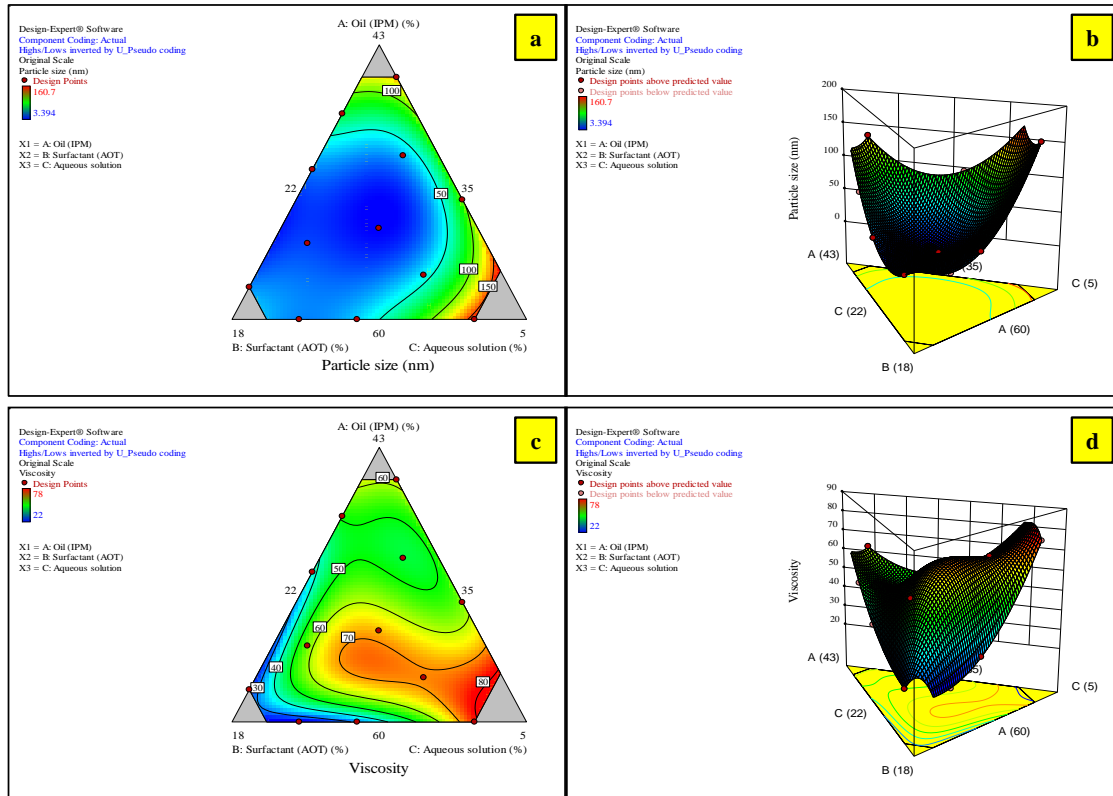


Figure 6.22. Box-Cox plots of (a) Particle size, (b) Viscosity, (c) pH and (d) % Drug release.

#### 4.2.4 Model Graphs

Figure 6.23 presents the contour and three-dimensional surface graphs for the evaluation of the effects of formulation components on response variables using Design Expert software. The contour plot and surface plot of globule size (Y1, Figure 6.23(a and b)) indicates that increase in the composition of surfactant and oil and decreased the composition of water led to decrease in particle size and better reduction of oil/water interfacial tension (Samson et al., 2016b). The effect of formulation components on viscosity (Y2) is shown in Figure 6.23(c and d). It was observed that increased oil content in microemulsion increased the viscosity. The surfactant has a synergistic effect on the viscosity because of the high probability of an increase of coalescence frequency between droplets (Samson et al., 2016b). Figure 6.23(e and f) show that formulation components have combined effects on pH. The contour and surface plot of % drug release (Figure 6.23(g and h)) indicates that drug release increases with an enhanced composition of

surfactant and decreasing the composition of water precursor( $\text{AgNO}_3$  and GA). Small droplets provide a large surface area for faster release of the drug. Surfactant increased the bioavailability, improve drug dissolution and increase the intestinal permeability (S. Gupta, Kesarla, & Omri, 2013).



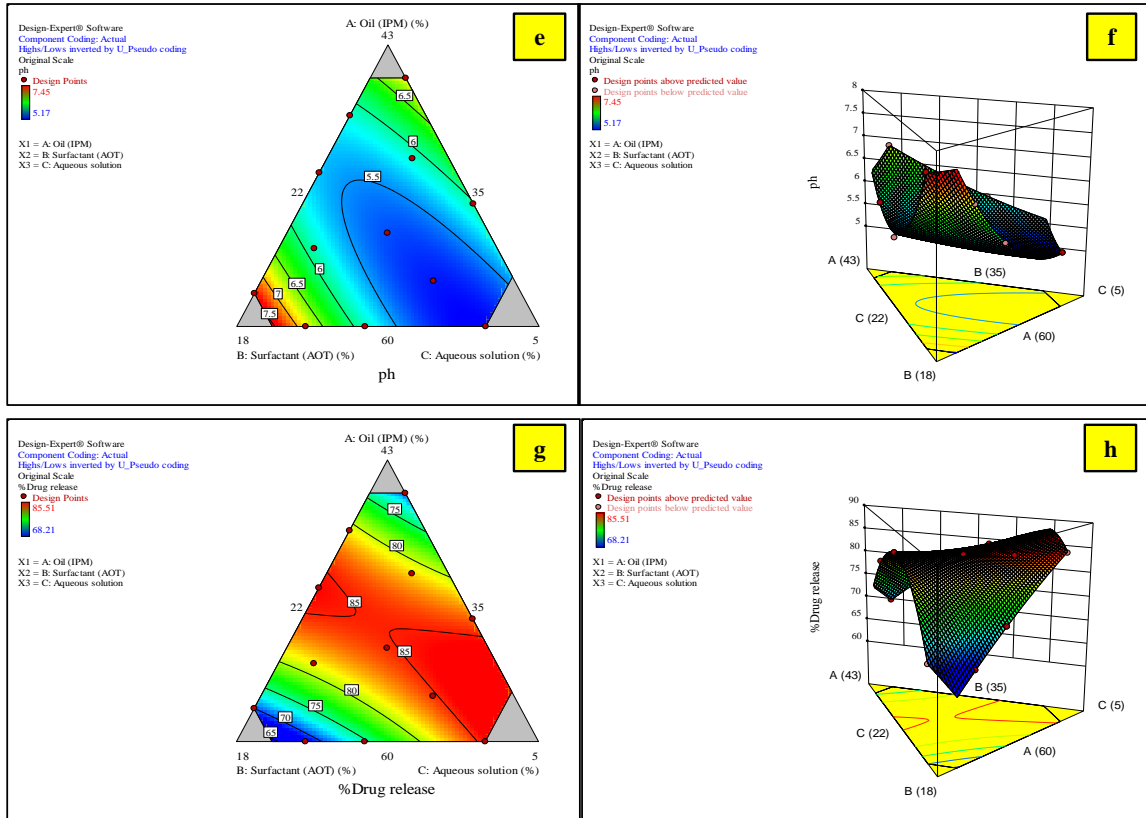


Figure 6.23. *Contour plots and 3-Dimentional response surface graphs describing the relationship of formulation variables with the responses, i.e. (a and b) Particle size, (c and d) Viscosity, (e and f) pH and (g and h) % Drug release.*

#### 4.2.5 Verification of experiment model

Table 6.12 lists the actual and model desired values of output variables for determining the accuracy of the experiment model. No significant difference was identified between the experimental and desired values of factors and response factors which give a close fit to the generated model and confirmed the model is validated.

Table 6.12 *The D-optimal Mixture Model Desired and Actual Values of Response Variables for AgNPs loaded ME*

Order	Y1 (Particle size)			Y2 (Viscosity)			Y3 (pH)			Y4 (%Drug release)		
	Actual Value	Predicted Value	Residual	Actual value	Predicted value	Residual	Actual value	Predicted value	Residual	Actual value	Predicted value	Residual
1	25.00	24.71	0.29	23.40	23.29	0.11	7.45	7.43	0.02	70.00	70.01	-0.013
2	37.00	36.31	0.69	31.60	31.39	0.21	5.83	5.84	-0.014	74.60	74.60	0
3	34.30	34.84	-0.54	47.00	46.89	0.11	5.87	5.87	0	80.81	81.54	-0.73
4	12.80	13.41	-0.61	56.80	56.68	0.12	5.92	5.87	0.045	81.28	81.46	-0.18
5	95.90	96.20	-0.30	57.00	57.06	-0.061	5.95	5.97	-0.015	84.00	83.69	0.31
6	71.00	73.30	-2.30	50.90	50.97	-0.075	5.92	5.86	0.063	81.20	80.99	0.21
7	135.40	134.20	1.20	47.00	46.89	0.043	6.86	6.87	-0.013	70.00	69.93	0.068
8	23.00	23.90	-0.90	22.00	22.29	-0.29	6.80	6.82	-0.024	68.21	68.16	0.048
9	41.77	42.30	-0.53	70.81	70.70	0.11	5.23	5.22	0.01	85.00	84.75	0.25
10	3.39	2.41	0.98	67.00	67.20	-0.20	5.37	5.34	0.025	85.00	84.81	0.19
11	160.70	160.53	0.17	78.00	78.04	-0.040	5.17	5.16	0.012	85.42	85.63	-0.21
12	25.71	23.87	1.84	40.01	37.04	-2.97	5.50	5.60	-0.10	85.51	85.46	0.051

Overlay plot (Figure 6.24) was produced by the graphical optimization technique which highlighted the area of optimization in the pseudo-ternary diagram with minimum and maximum limits of the response variables and optimized formulation variables.

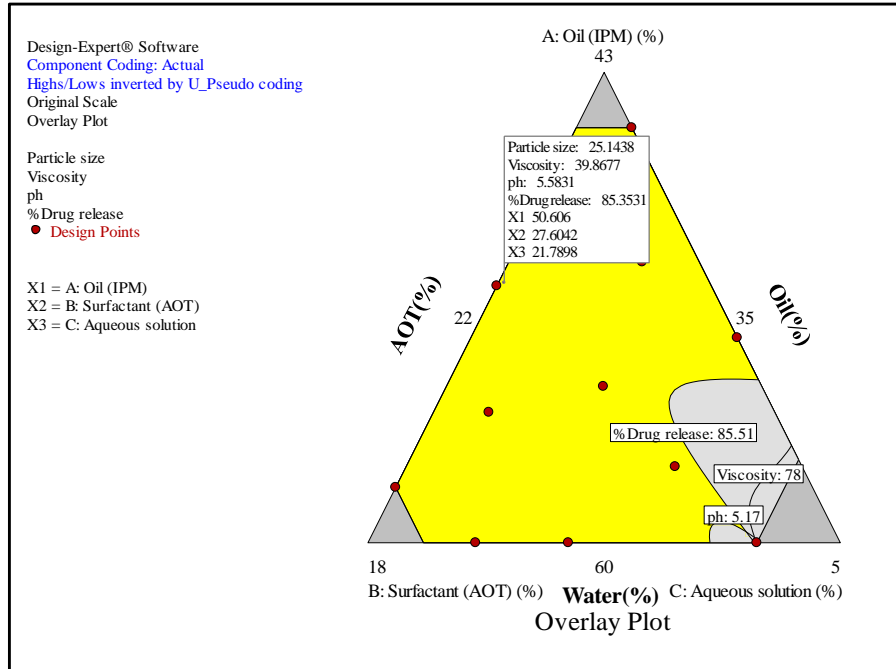


Figure 6.24. Overlay plot of optimized formulation composition and predicted response values.

As observed in Figure 6.24 the predicted microemulsion formulation contained 50.606% oil, 27.604% Surfactant, and 21.79% water and the particles size, viscosity, pH and %Drug release was obtained as 25.15, 39.87, 5.58 and 85.35 respectively which were in close agreement with the optimized Formulation no. 12 values (Table 6.13).

Table 6.13 *The Actual and Model-Predicted Composition and Response Values for Optimized Formulation*

<b>Composition (%)</b>	<b>Predicted</b>	<b>Actual</b>	<b>Response</b>	<b>Predicted</b>	<b>Actual</b>	<b>RES %</b>
<b>Oil (IPM)</b>	50.606	50.710	<b>Particle size</b>	25.15	25.71	2.18
<b>Surfactant (AOT)</b>	27.604	27.290	<b>Viscosity</b>	39.87	40.01	0.35
<b>An aqueous solution of (silver and Gallic acid)</b>	21.79	22.00	<b>pH</b>	5.58	5.51	1.25
			<b>% Drug release</b>	85.35	85.51	0.18

### 4.3 Characterization techniques of optimized AgNPs loaded ME

#### 4.3.1 UV-visible absorption spectral analysis

Figure 6.25 presents the UV-Vis spectra of GA and AgNPs loaded ME. The spectrum shows a sharp plasmon absorption peak at 410 nm, which confirmed the synthesis of well-dispersed AgNPs in ME. It indicates that the binding of GA with silver resulted in a red shift of the absorption band of loaded AgNPs at 410 nm.

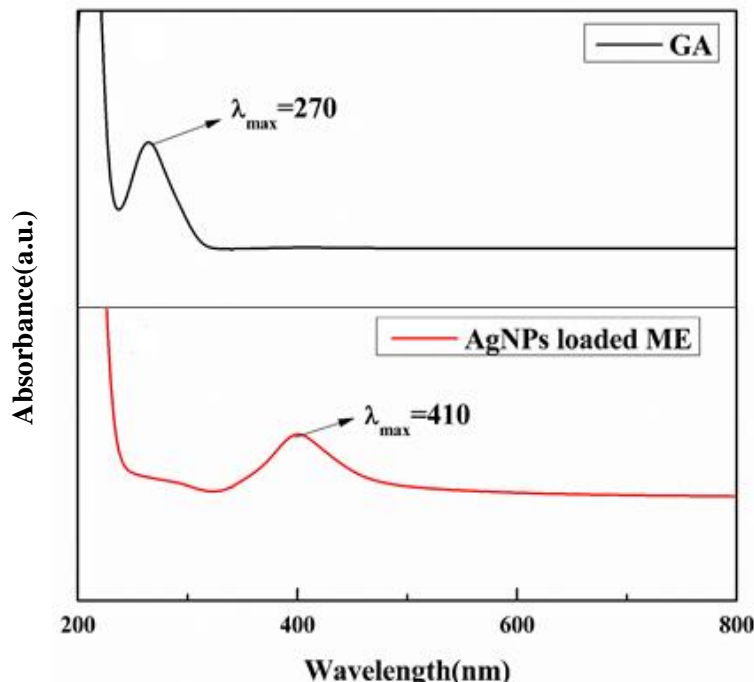


Figure 6.25. UV-Vis absorption maxima of (a) GA and (b) optimized AgNPs loaded ME formulation.

#### 4.3.2 Globular Size and dispersity Index (PDI)

The globular size of microemulsion was observed in a range of 3-160nm (Table 6.8). The PDI of microemulsion was found between 0.2 - 0.5, which confirms the monotonous distribution of globules. The globular size of optimized formulation was found 25.71 with PDI 0.3 which confirmed the uniform distribution of particles (Figure 6.26).

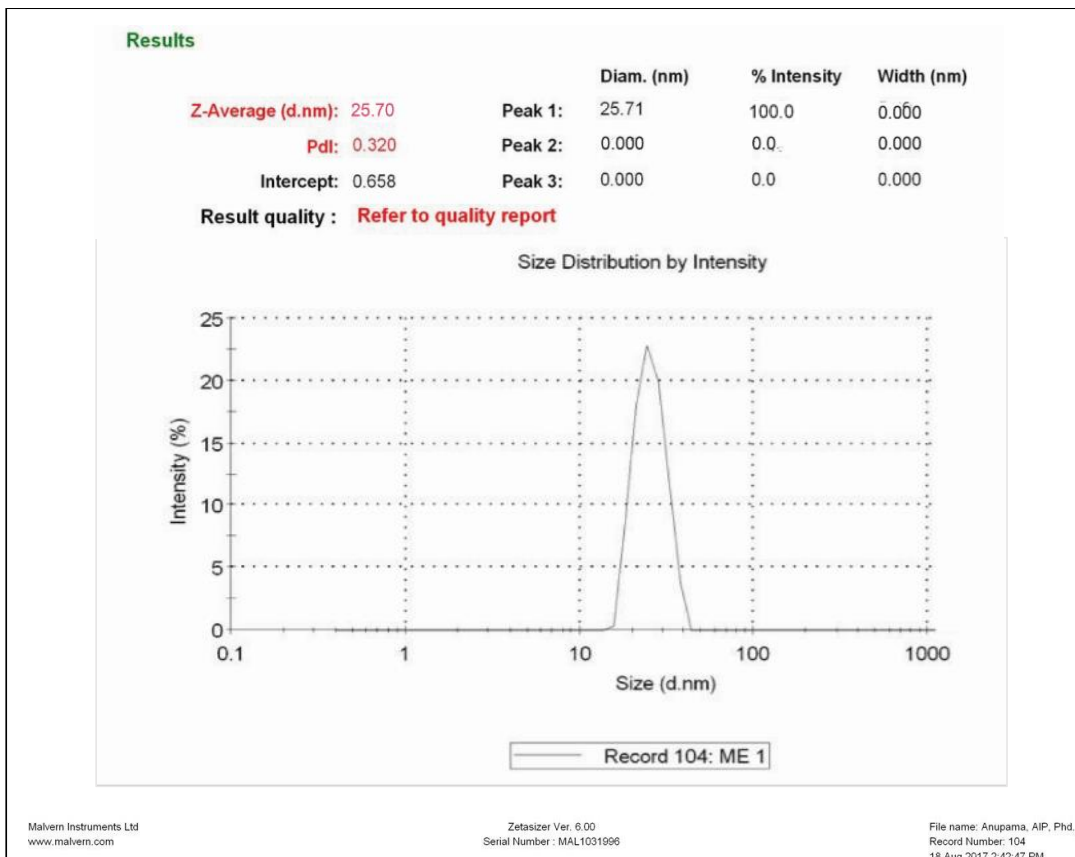


Figure 6.26. DLS report of optimized AgNPs loaded ME formulation.

#### 4.3.3 Transmission electron microscopy (TEM)

The TEM picture and size distribution histogram in Figure 6.27 shows the morphological characteristics of optimized microemulsion formulation. As shown in Figure 6.27 water globule with a diameter 10-25nm are spherical in shape. This study confirmed that the microemulsion droplet are spherical and size distribution in narrow range.

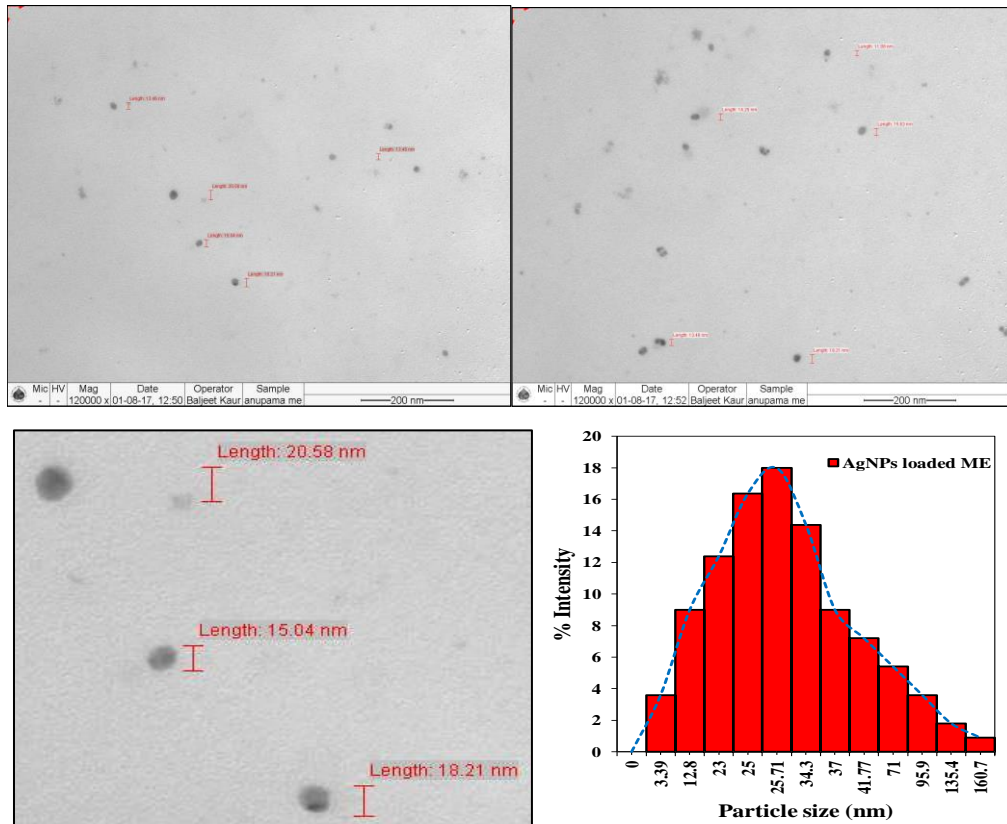


Figure 6.27. TEM images at lower and higher magnification of 12000 x and size distribution histogram of AgNPs loaded ME.

#### 4.3.4 Viscosity, pH and Conductivity

The viscosity or thickness of *w/o* ME was found in the range of 22 to 70 cp at 100 rpm. Table 6.8 presents the pH of formulations were measured in the range of 5 to 7. For oral administration, this pH value could come within the approval range. The value of pH and viscosity of optimized formulation was found  $5.5 \pm 0.05$  and  $40.01 \pm 0.1$  cp respectively. The conductivity of optimized formulation was found  $15.01 \pm 0.1 \mu\text{S}$ , which confirms the synthesis of *w/o* microemulsions. Generally *o/w* microemulsion have large conductivity because water is in external phase; with increase in water concentrations, conductance of ME system also increases because of increase of conductive ion per unit volume (R. Kumar, Kumar, & Sinha, 2016).

#### 4.3.5 Density

The density of optimized formulation was found  $0.891 \pm 0.21 \text{ g/cm}^3$ . The higher of surfactant in the microemulsion formula, it will increase the density of the formulation.

From the results of measurement of density, showed that the density of the optimized formulation can flow properly and easily pourable.

#### **4.3.6 Surface tension measurement**

Surface tension measurements determines the stability of AgNPs loaded ME formulation. Surface tension of optimized *w/o* microemulsion was found  $29.8 \pm 0.057$  dynes/cm. This low value of surface tension requires low energy to enhance the surface area so that decrease the interfacial surface tension among oil and water droplets and dispersion occurs (micro-emulsification) easily and the formulation is thermodynamically stable. The addition of surfactants will cause a decrease in surface tension, the surface tension at a certain concentration will be constant even if the surfactant concentration increased. Due to the water droplets surrounded by a continuous oil phase in *w/o* microemulsion, the surface tension of ME is close to the oil phase which confirms the formation of *w/o* microemulsions.

#### **4.3.7 Zeta potential determination**

Zeta potential study was analyzed for determining the longer storage stability of formulations and particle surface charge (Pan et al., 2013). Figure 6.28 indicates the zeta potential measurement of optimized formulation was found  $-0.361$  mV with conductivity  $0.015$  mS/cm. Due to the increased negative surface charge, electrostatic energy slows down the coagulation of nanoparticles in microemulsion and remain stable for months. Low surface charge of nanoparticles in microemulsion droplets increased membrane permeability of particles in the cancers cell resulting improved anticancer potential.

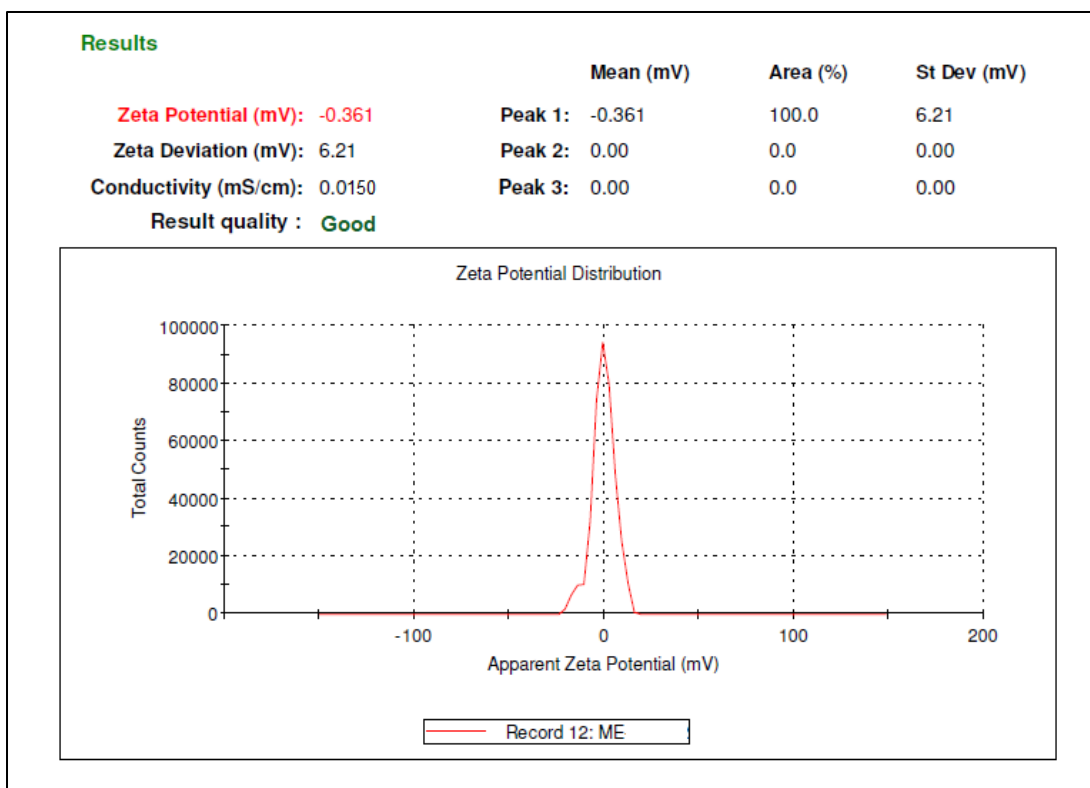
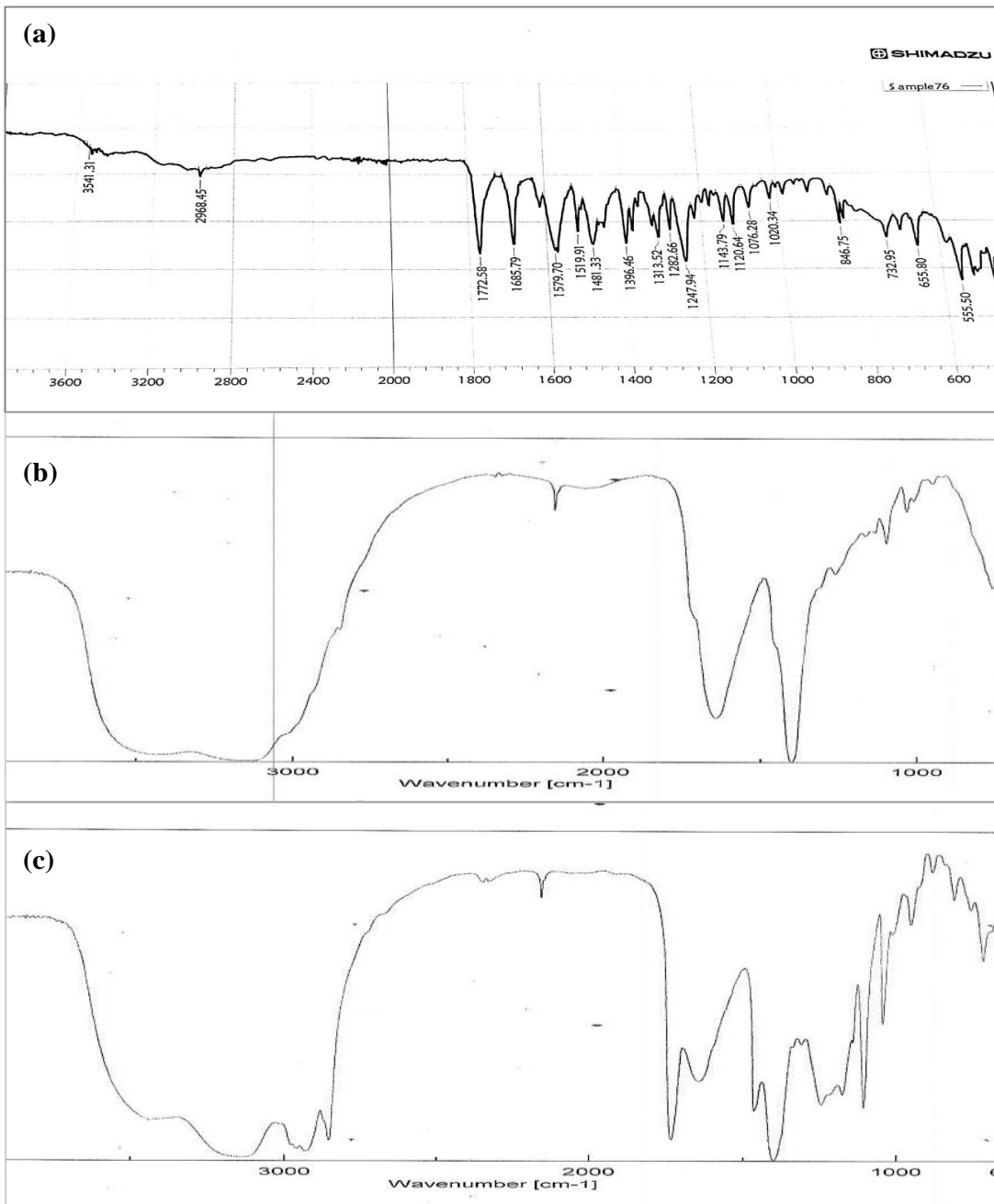


Figure 6.28. Graphical representation of Zeta potential of optimized AgNPs loaded ME formulation.

#### 4.3.8 Fourier transform infrared (FTIR) analysis

FTIR study is an essential tool for identifying functional groups of GA and AgNPs or possible atoms or molecules which is responsible for the reaction mechanism of silver ions and synthesis of AgNPs loaded microemulsion (Theivasanthi & Alagar, 2013b). Figure 6.29(a and b) represents the FTIR spectra of the GA standard and excipients mixture respectively. The infrared spectrum changed upon the synthesis of AgNPs loaded microemulsion (Figure 6.29c). Figure 6.29a indicates a broadband peak between 3600 and 2510 cm<sup>-1</sup> and the sharp-edge peak at 1772 cm<sup>-1</sup> because of the vibration of O-H(alcohol) group stretching and a C-O, which confirms the presence of carboxyl group in the GA. This carboxyl group binds to the surface of the AgNPs (W. Wang et al., 2007b). These bonds completely disappeared after the synthesis. The absorption peak recorded at 1685, 1579, and 1481 cm<sup>-1</sup> was because of the vibration stretch of Carbon–Carbon bonds in an aromatic group (W. Wang et al., 2007b). Various peaks observed in 1300–1000 cm<sup>-1</sup> region corresponded to C–O stretch vibration and O–H bond bending vibration of phenolic GA (W. Wang et al., 2007b). In Figure 6.29(b), the band was shown in the

3600–2700  $\text{cm}^{-1}$  band was due to the O-H group stretching vibration indicating the presence of alcohol and phenol, which covered C–H bond at about 3100  $\text{cm}^{-1}$  due to aromatic compounds stretching vibration (W. Wang et al., 2007b). The band observed in 1300–1000  $\text{cm}^{-1}$  region of stretch vibration of C–O and O–H bending vibration was still retained, but the intensity reduced. Figure 6.29c presents the FT-IR spectra of AgNPs loaded ME. It indicates that C–O bond of stretching vibration adjusted from 1722 to 1634  $\text{cm}^{-1}$ , and the C–C bond shift at 1685 and 1579  $\text{cm}^{-1}$  due to stretching vibration changed in a broad band at intensity 1634  $\text{cm}^{-1}$ . Figure 6.30c presents the absorption band recorded at 3407  $\text{cm}^{-1}$  for AgNPs loaded ME confirms the presence of intermolecular hydrogen bonds of phenolic groups on the exterior of the NPs. The adjustment in the IR bands resulting the reaction of silver ions with excipients and synthesis of NPs in microemulsion.



*Figure 6.29.* FTIR spectrum recorded by making KBr disc of (a) GA standard (b) Excipients mixture and synthesized (c) AgNPs loaded Microemulsion.

#### 4.3.9 Refractive Index

The RI of the optimized AgNPs loaded microemulsions was found  $1.43 \pm 0.01$  which was so close to the oil's RI of 1.435. It confirmed the isotropic nature of *w/o* microemulsion (R. Kumar et al., 2016).

#### 4.3.10 Rheological behavior measurements

The rheological study or flow properties represents that the viscosity is very low of all the *w/o* Microemulsions. Figure 6.30(a and b) presents the rheological graph indicates that all formulation systems represents a Newtonian flow materials with linear connection between the shear stress and shear rate (Silva, Barratt, Chéron, & Egito, 2013). In conclusion, formulation systems are acceptable for oral drug administration because of low viscosity.

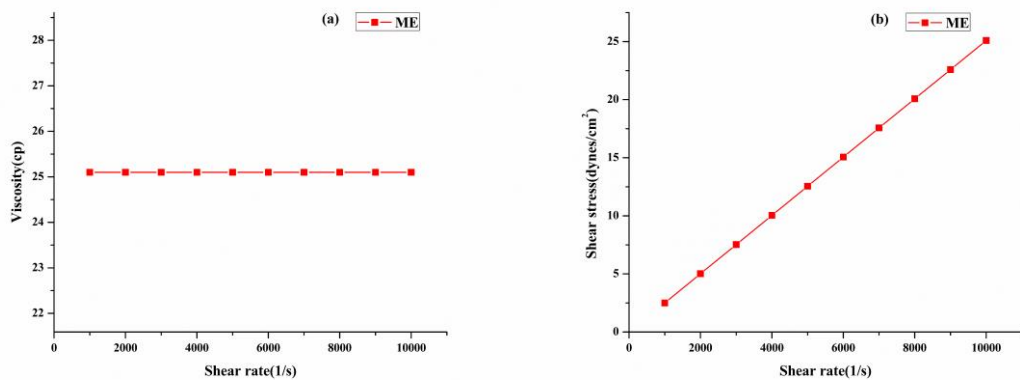


Figure 6.30. Linear graph of viscosity or shear rate (a) and shear stress as a function of shear rate for AgNPs loaded ME (b).

#### 4.4 Drug content (DC) and Entrapment efficacy (EE) of GA

The Gallic acid drug content in optimized AgNPs loaded Microemulsion was found to be  $95.23 \pm 0.25\%$  (mean  $\pm$  SD,  $n=3$ ). The % EE was found  $90 \pm 0.25\%$ . It is concluded that GA was uniformly distributed throughout the microemulsion and drug loss was minimum during the synthesis of the formulation.

#### 4.5 Inductively coupled plasma-mass emission spectroscopy (ICP-MS)

The ICP-MS spectroscopy was studied to measure the Ag ion concentration used for reduction by GA to obtain AgNPs in microemulsion. Ag was measured in this solution by ICP-MS to determine the total Ag content whereas  $0.81 \pm 0.42$  ppm (Figure 6.31) of Ag was found in the microemulsion, accounting for 72.9% of the total amount of Ag released from formulation.

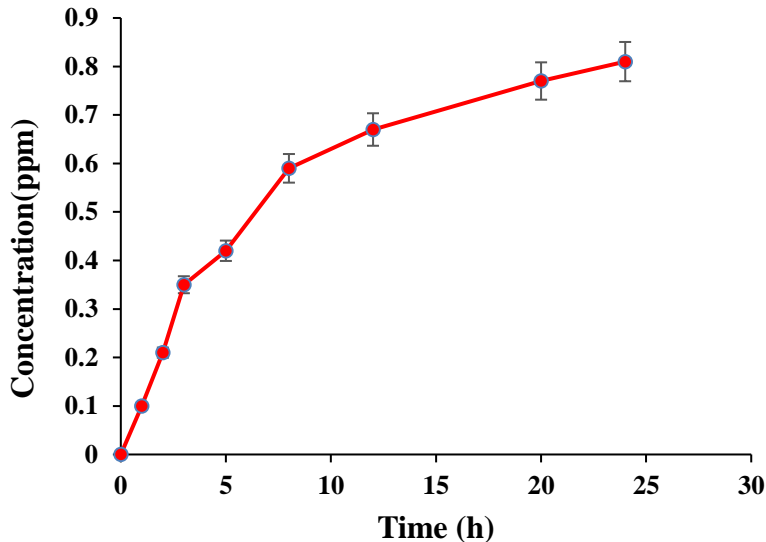


Figure 6.31. ICP-MS of silver in AgNPs loaded ME.

#### 4.6 *In-vitro* release study

Figure 6.32 presents the *in-vitro* release study of the optimized formulation. It is observed that  $85.51 \pm 0.05\%$  drug release was achieved at target cancer cell pH 5 in compare to the systematic pH 7.4 in which drug release were observed to be  $68.5 \pm 0.02\%$  over the period of 24 h. Optimized microemulsio showed a burst release of the drug at the initial stage and then exhibited an extended release over the 24h. The slowest drug release was observed at blood system pH of 7.4, and the highest release was identified in pH 5, which is the pH of cancer cells. It is concluded that the formulated microemulsion can be used as an effective drug delivery system for targeting cancer because of its pH-sensitive properties.

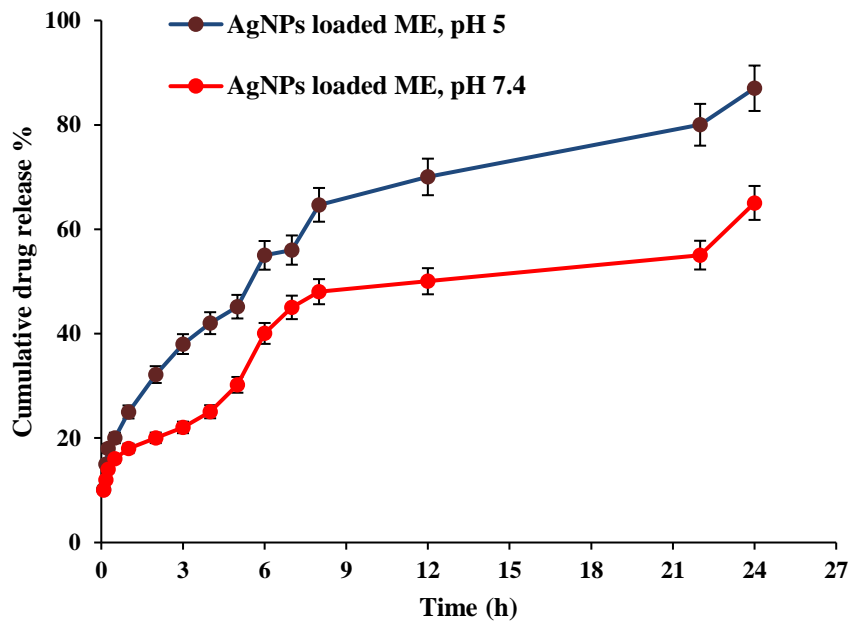
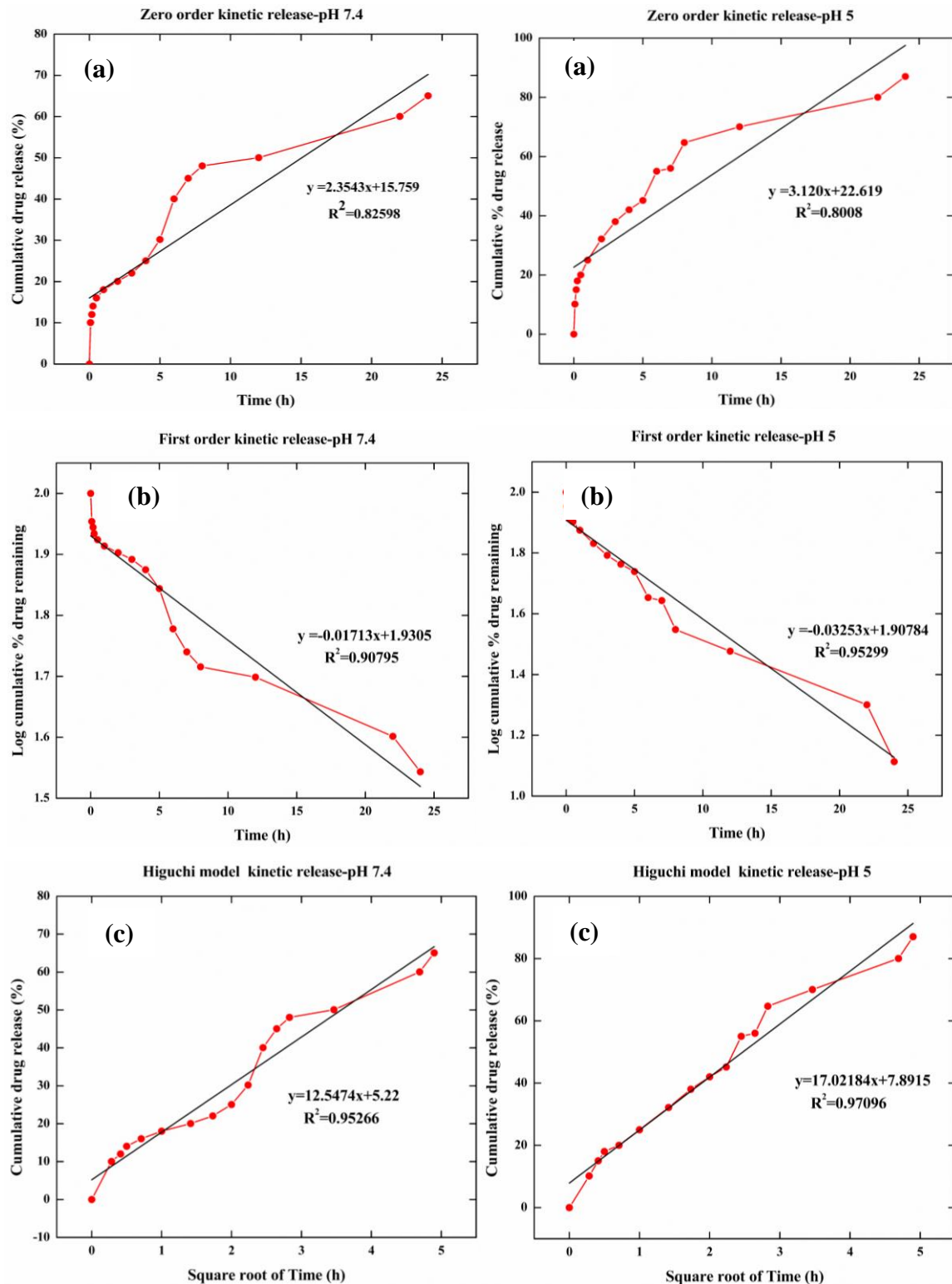


Figure 6.32. GA *in-vitro* release graph of AgNPs loaded ME in cancer cell acetate pH 5 and PBS pH 7.4. Result was presented as mean $\pm$ SD (n=3)

#### 4.7 Release kinetic study

Based on the kinetic analysis (Figure 6.33 and Table 6.14) it was observed that the release of drug from AgNPs loaded ME followed the Higuchi model at systematic pH 7.4 and cancer cell pH 5. The ‘n’ values of 1.3 and 1.4, the Korsmeyer-peppas equation suggested that the drug follows the controlled release behavior which is a super case II release kinetics. These results indicate that the drug was released by diffusion. Drug release from such matrices may be controlled by erosion, or drug diffusion, or by these processes altogether.



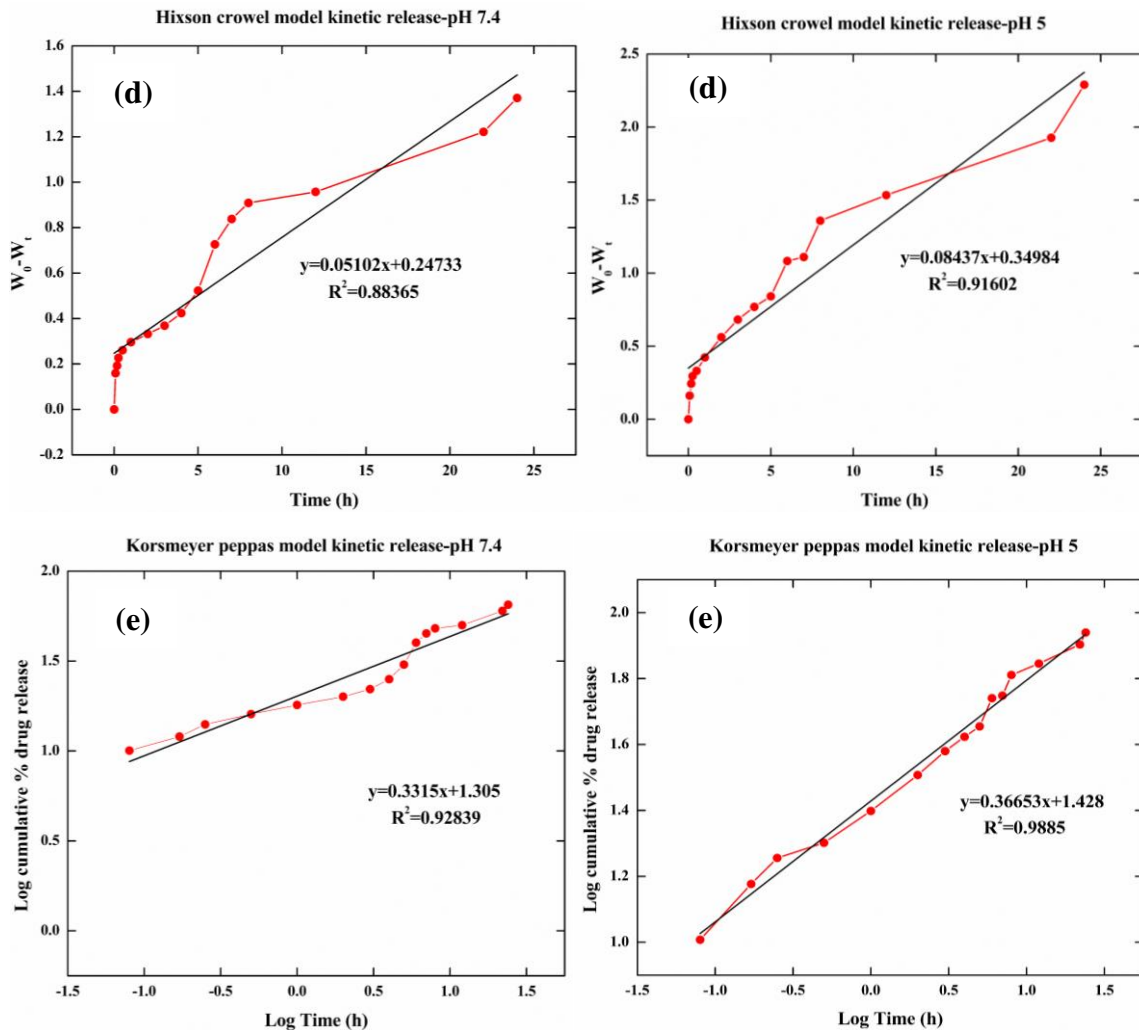


Figure 6.33. Graphical representation of drug release kinetics mechanism of optimized AgNPs loaded ME formulation at (a-e) pH 7.4 and (a-e) pH 5 for Zero model, Ist model, Higuchi, Hixson and Korsmeyer-peppas model.

Table 6.14 *Release Kinetics and Their Parameters*

Kinetic model	Zero-order reaction model	Ist order reaction model	Higuchi reaction model	Korsmeyer-Peppas reaction model	Hixon crowel reaction kinetic model
	k R <sup>2</sup>	k R <sup>2</sup>	k R <sup>2</sup>	n R <sup>2</sup>	k R <sup>2</sup>
pH 7.4	2.25 0.8259	0.016 0.9079	12.14 0.9526	1.3 0.9283	0.051 0.8837
pH 5	6.62 0.8008	0.032 0.9529	17 0.9790	1.42 0.9885	0.0844 0.916

## 5 Antimicrobial study of optimized AgNPs in BNCs and AgNPs loaded ME formulations

Figure 6.34 and 6.35 presents the antibacterial assay of different concentration of AgNPs in BNCs (0.5, 1, 2, 5, 6, 8, 10 and 15 µg/ml and AgNPs loaded ME (0.5, 1, 2, 5, 10, 20, 25 and 100 µg/ml) respectively was evaluated against bacterial strains (Gram+; *S. aureus*), Gram-; *P. aeruginosa* or *E. coli*) and fungus (*Candida albicans*). Table 6.15 presents the results of MICs with ZOIs of the optimized AgNPs in BNCs and AgNPs loaded ME formulations against the bacteria's *E. coli*, *S. aureus*, *P. aeruginosa* and fagus *C. albicans*. At concentration 5 µg/ml and above, the AgNPs in BNCs and AgNPs loaded ME formulations showed a clear ZOI area. No zone of inhibition was found in the vehicle control well which confirmed that the inhibition in bacteria and fungus was specifically due to AgNPs. The obtaining responses determines that the synthesized AgNPs in BNCs and in w/o microemulsion have promising antibacterial potential against microorganisms. There are various mechanisms for interacting AgNPs with microbes and damage them. The mechanism of silver NPs inhibiting antimicrobial growth depends on its binding to microbial cell surface membrane. Nanoparticles with having large surface area interfere with bacteria's function, disrupt its mitochondrial membrane and producing a potential bactericidal effect (Guzman, Dille, & Godet, 2012).

Table 6.15 *MICs with a Zone of Inhibition against Pathogenic Bacteria of AgNPs loaded ME Data was shown in triplicate (n=3), (mean ± SD)*

<b>Bacteria's</b>	<b>AgNPs in BNCs</b>		<b>AgNPs loaded ME</b>	
	<b>*MIC (µg/ml)</b>	<b>*ZOI (mm)</b>	<b>MIC (µg/ml)</b>	<b>ZOI (mm)</b>
<b>Gram+ <i>Escherichia coli</i> (MTCC1687)</b>	5	8.47±0.12	13.62±0.21	5
<b>Gram-<i>Staphylococcus aureus</i> (MTCC737)</b>	6	9.34±0.25	11.24±0.11	5
<b>Gram- <i>Pseudomonas aeruginosa</i> (MTCC1688)</b>	5	8.8±0.15	12.55±0.41	5
<b>Fugus <i>Candida albicans</i>(MTCC227)</b>	5	11.08±0.32	13.15±0.31	5

\* MIC: Minimum inhibitory concentration; \*ZOI: Zone of inhibition

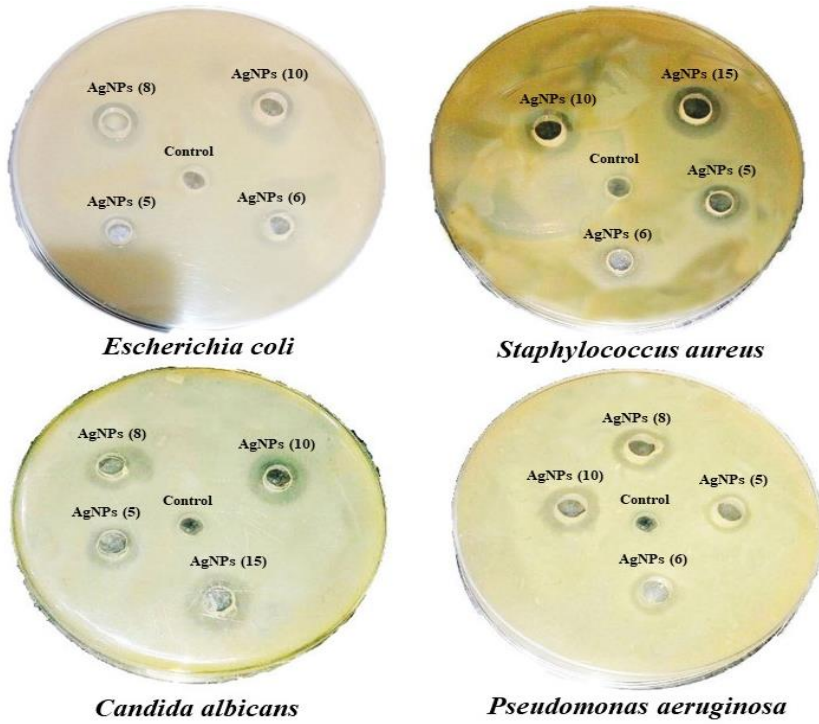


Figure 6.34. Antimicrobial activity of optimized AgNPs in BNCs various concentrations against bacteria and fungus.

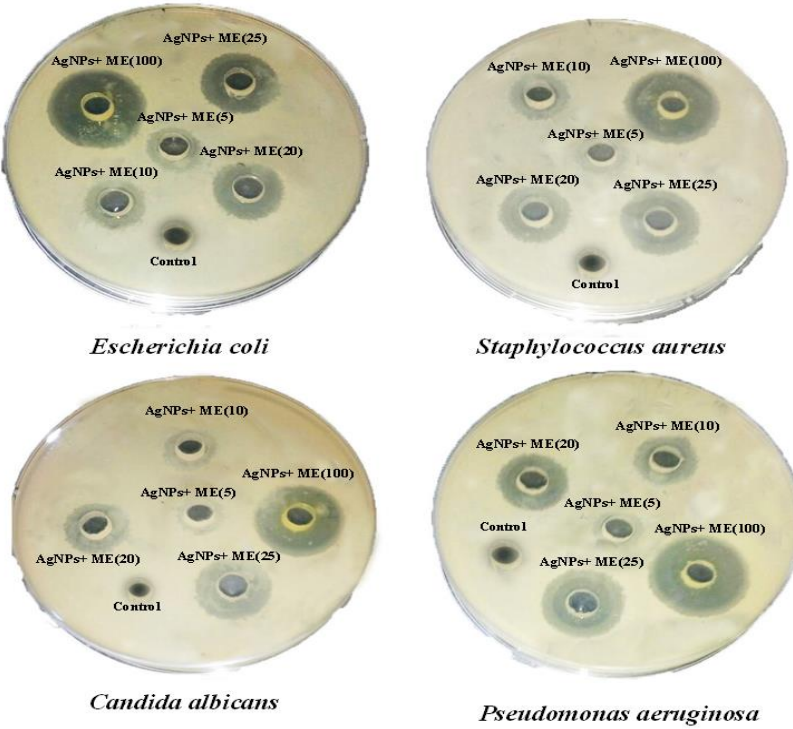


Figure 6.35. Antimicrobial activity of AgNPs loaded ME's different concentrations against bacteria and fungus.

## 6 In-vitro Anticancer study by MTT assay

In this research, MTT procedure was used to evaluate the cytotoxic assay of synthesized AgNPs and AgNPs loaded ME on MCF-7 cancer cells and compared with the control. From the MTT assay, it was determined that the cytotoxicity against BC cell line enhanced with increasing concentration of AgNPs and AgNPs loaded ME (Figure 6.36). The proliferation of MCF-7 cancer cell line treated with AgNPs and AgNPs loaded ME was significantly inhibited in a dose-dependent manner, concerning control cells ( $p<0.001$ ), GANPs (80  $\mu\text{g/ml}$ ) and standard drug CPT (15 $\mu\text{M}$ ) ( $p<0.01$ ). The IC<sub>50</sub> of AgNPs (a) and AgNPs loaded ME (b) was detected at  $22.5 \pm 0.021$  and  $16.72 \pm 0.014 \mu\text{g/ml}$  respectively against the MCF-7 cancer cell lines (Figure 6.37).

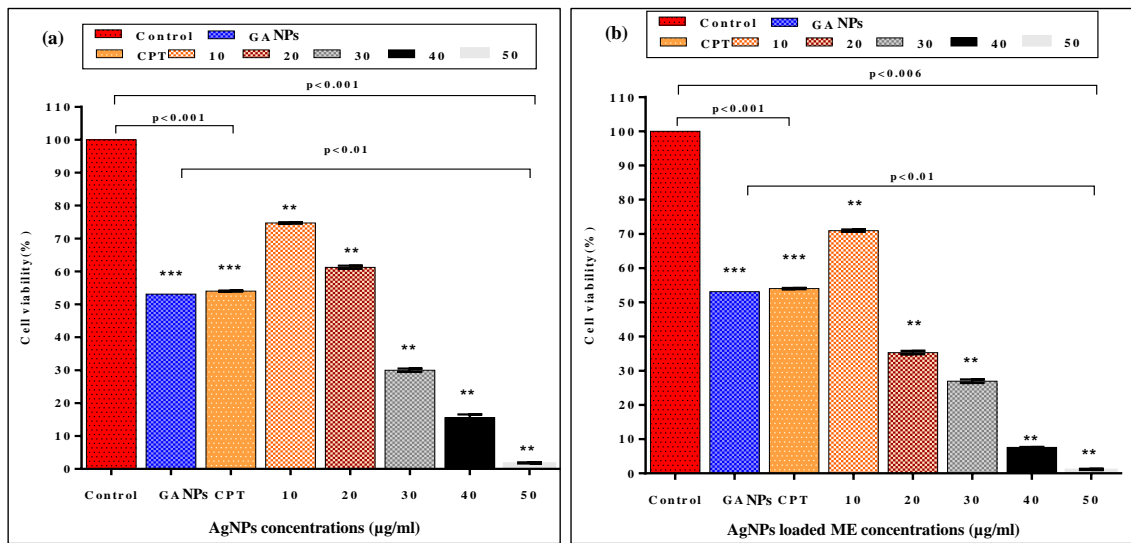


Figure 6.36. In vitro anticancer activity of different concentrations of (a) AgNPs in BNCs and (b) AgNPs loaded ME on MCF-7 cancer cell line. Camptothecin (CPT) 15 $\mu\text{M}$  dose concentration was used as a standard anticancer drug.

Results were represented as mean  $\pm$  SD with two experiment. \*\*\* $p<0.001$  MCF-7 control vs. CPT. \*\*\* $p<0.001$  MCF-7 control vs. GANPs (80.2  $\mu\text{g/ml}$ ). \*\* $p<0.01$  AgNPs loaded ME vs. GANPs. \*\*\* $p<0.006$  control vs. AgNPs and AgNPs loaded ME. \*\* $p<0.01$  AgNPs loaded ME vs. CPT.

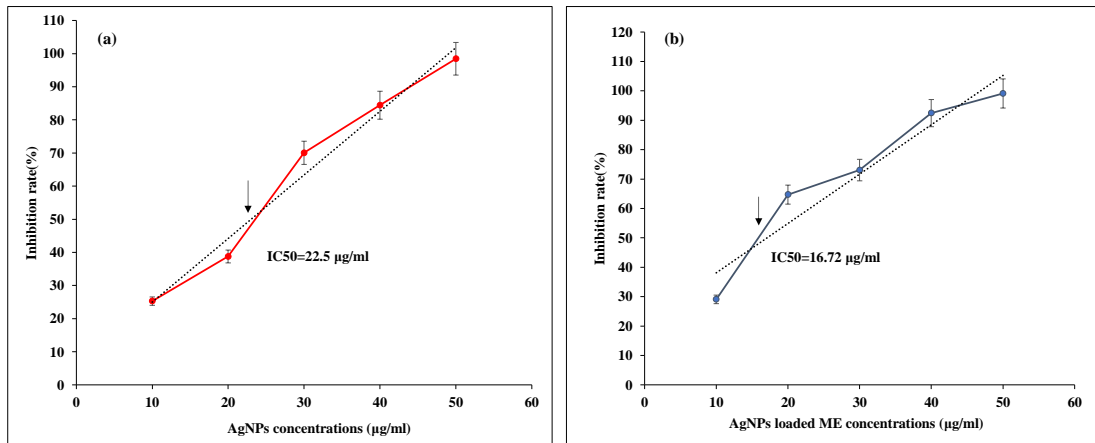


Figure 6.37. Graphical representation of IC<sub>50</sub> value of (a) AgNPs in BNCs and (b) AgNPs loaded ME against MCF-7 cancer cell line.

MCF-7 cancer cells treated with IC<sub>50</sub> of formulations for 24 h resulted in 50% inhibition of cells compared to untreated control. Figure 6.38 presents the morphological evaluation of control cells, the IC<sub>50</sub> concentration of microemulsion and standard drug CPT treated cancer cells. From the morphological analysis of formulations treated cancer cells structural changes like cell contraction, changes in membrane surface and inhibition of cell growth was observed. It is confirmed that apoptosis has been induced in AgNPs and AgNPs loaded ME treated MCF-7 cancer cells.

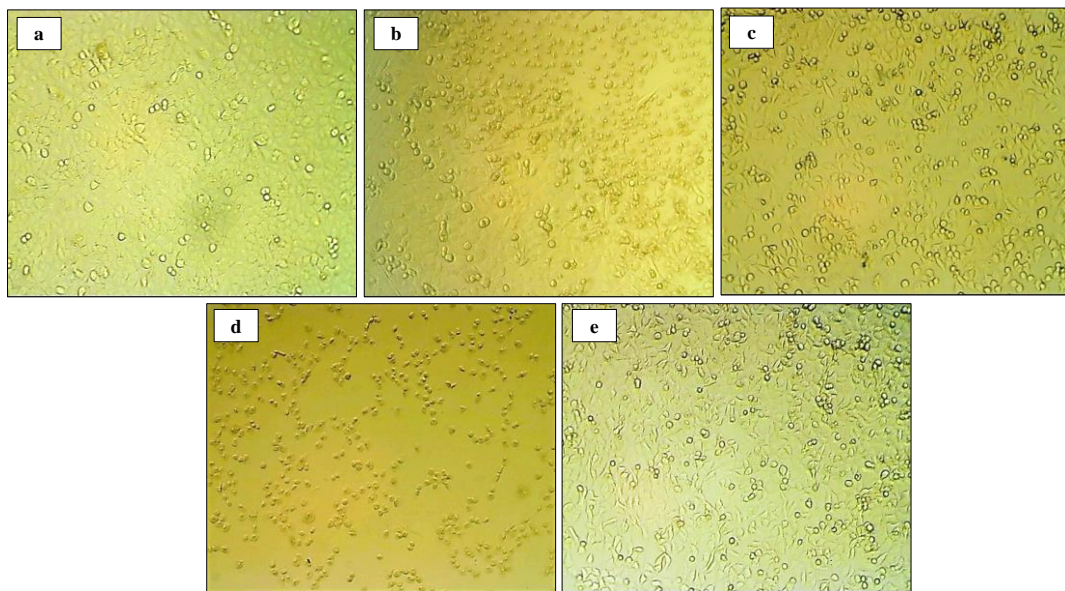


Figure 6.38. Morphology assessment of (a) MCF-7 control, IC<sub>50</sub> of (b) AgNPs in BNCs (22.5  $\mu\text{g/ml}$ ), (c) AgNPs loaded ME treated (16.7  $\mu\text{g/ml}$ ), (d) GANPs treated (80.2  $\mu\text{g/ml}$ ) and (e) Camptothecin (CPT, 15  $\mu\text{M}$ ) treated cancer cell line.

## 7 In-vivo Antitumor study

### 7.1 Ehrlich solid tumor volume (TV) and mice body weight (BW)

The average TV of EAC disease control mice gradually increasing from  $100.12 \pm 0.68 \text{ mm}^3$  to  $1258.20 \pm 63 \text{ mm}^3$  after 21 days (Figure 6.39). The tumor volume was found to be reduced from  $99.22 \pm 4.25 \text{ mm}^3$  to  $350 \pm 70.04 \text{ mm}^3$  received oral treatment of AgNPs loaded ME and  $97.50 \pm 2.87 \text{ mm}^3$  to  $370.26 \pm 70.14 \text{ mm}^3$  received oral treatment of AgNPs in BNCs as contrast to the EAC disease control ( $p < 0.001$ ) and GANPs group ( $400.7 \pm 33.73 \text{ mm}^3$ ), which is close to the standard Methotrexate group ( $320.2 \pm 75.71 \text{ mm}^3$ ). These results determine that the rapid reproduction of EAC cells in treated groups were reduced by AgNPs in BNCs and AgNPs loaded ME due to a decrease in the weight of solid tumor after 21 days (Figure 6.40). The quantitative weight of solid tumor treated with AgNPs in BNCs and AgNPs loaded ME was also found smaller ( $p < 0.001$ ) and confirmed significant tumor growth inhibition in compared to EAC control mice (Figure 6.39, Table 6.16). The BW changes were found significantly increasing in AgNPs in BNCs and AgNPs loaded ME treated groups in compared to EAC disease control and GANPs treated groups (Figure 6.40b and c). It confirmed the effect of AgNPs in BNCs and AgNPs loaded ME treatment in preventing the tumor growth which is close to standard group.

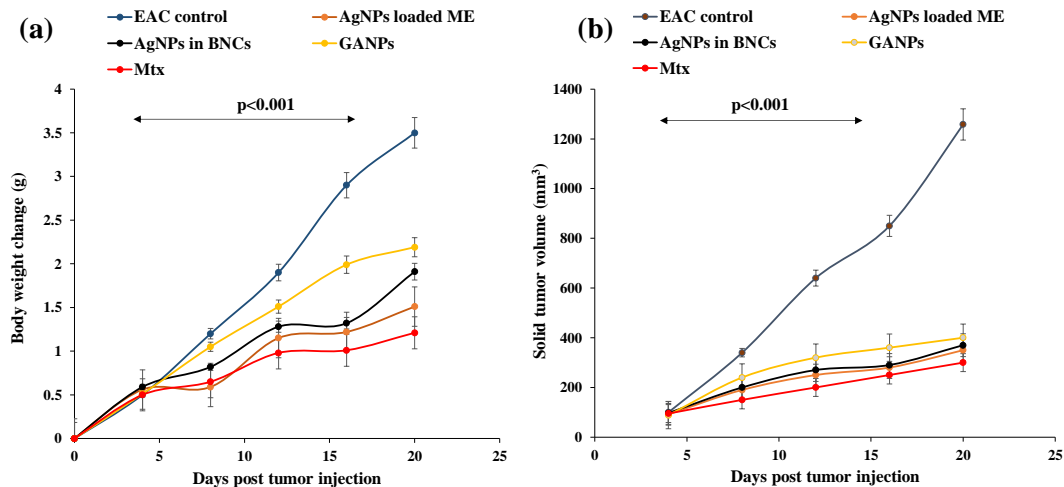


Figure 6.39. Effect of formulations on (a) Body weight changes and (b) Tumor volume in EAC solid tumor mice. The results were shown as mean $\pm$ SD ( $n = 6$ ) ;  $p$  value was found  $< 0.001$  was compared to EAC control.

Table 6.16 *Effect of Formulations on the Tumor Weight and % Tumor Inhibition of EAC Solid Tumor Control (n=6)*. \*\*\**p* value was found < 0.001 in compared to EAC Tumor Control

Groups	*TW (g)	*(%TIR)
EAC control	3.50±1.21	-
AgNPs loaded ME	1.51±1.55***	72.16***
AgNPs in BNCs	1.91±1.31***	70.58***
GANPs	2.19±2.21***	68.20***
Mtx	1.21±1.01***	76.16

\*TW: Tumor weight; \*TIR: Percent tumor inhibition rate

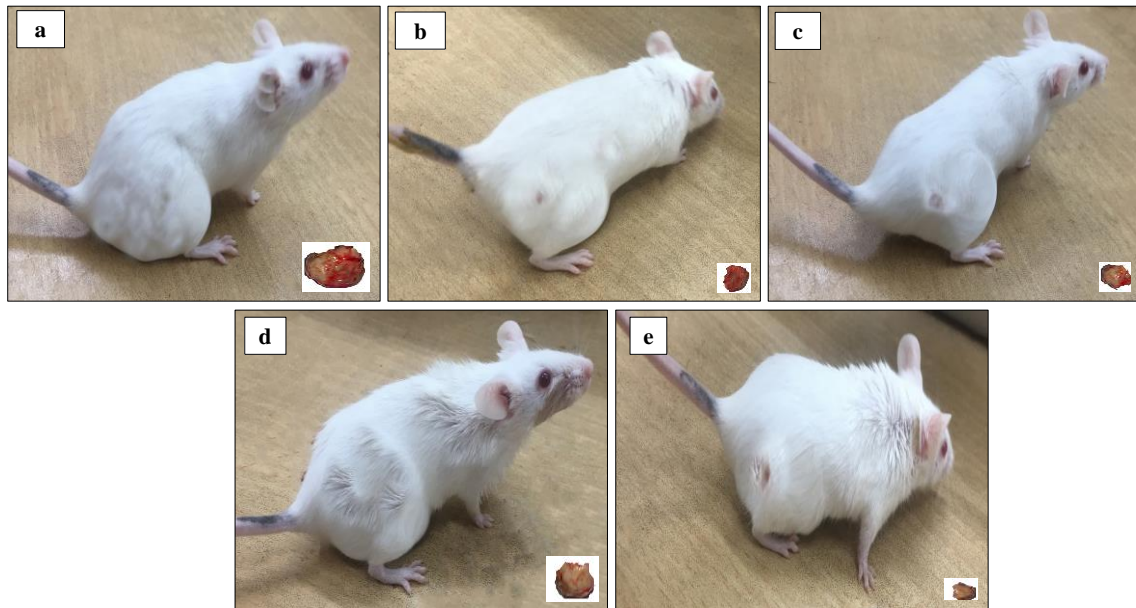


Figure 6.40. Solid tumor appearance in (a) EAC control, (b) AgNPs loaded ME treated, (c) AgNPs in BNCs treated, (d) GANPs treated and (e) Mtx treated mice after 21 days.

## **7.2 Effects on Hematological parameters**

Hematological or blood parameters of all tumor-bearing mice were evaluated after 15 days before starting the experiment is presented in Table 6.17. A decreased count of hemoglobin and RBCs was noticed in Ehrlich ascites disease control group in contrast to the positive control group due to the iron deficiency (Sreelatha, Padma, & Umasankari, 2011). AgNPs loaded ME and AgNPs in BNCs treated groups elevated the level of hemoglobin and RBCs as close to the normal control and standard. A negligible, increased level of hemoglobin and RBCs was observed in GANPs treated mice compared to AgNPs loaded ME treated group. An increase WBCs count was observed in Ehrlich ascites disease control group in compare to the positive mice control group. AgNPs loaded ME and AgNPs in BNCs treatment groups observed with lack of WBC count in contrast to the Ehrlich ascites disease control group. In a total leucocyte count, it is confirmed that the increased counts of lymphocytes, monocytes, and neutrophils was observed in EAC disease control group in contrast to the positive control. It might be because of the rapid proliferation of tumor cells in disease control mice. AgNPs loaded ME and AgNPs in BNCs treated groups restores these leucocytes count as close as normal or standard Methotrexate (Mtx) group. While the decreased level of neutrophils was observed in AgNPs loaded ME and AgNPs in BNCs treated groups in contrast to the Ehrlich ascites control. Platelets count was increased in AgNPs loaded ME and AgNPs in BNCs treatment groups in contrast to the EAC disease control group. The hematological parameters confirmed that AgNPs loaded ME and AgNPs in BNCs induce the protective behaviour on the hematogenic system without developing toxicity to blood cells.

Table 6.17 *Hematological Parameters of Untreated and Treated Mice. Data was shown as (n=6., mean $\pm$ SD)*

<b>Parameters</b>	<b>Normal control</b>	<b>EAC disease control</b>	<b>AgNPs loaded ME</b>	<b>AgNPs in BNCs</b>	<b>GANPs</b>	<b>Mtx</b>
Hemoglobin (g/dL)	14.09 $\pm$ 1.0	9.12 $\pm$ 0.03 ***	13.08 $\pm$ 0.1 1*** <sup>a</sup>	10.17 $\pm$ 0.8 0*** <sup>\$</sup>	9.60 $\pm$ 0.39 ***	12.12 $\pm$ 1.0 0*** <sup>b</sup>
RBC( $10^6$ /m m <sup>3</sup> )	4.68 $\pm$ 0.32	3.11 $\pm$ 0.90 ***	3.93 $\pm$ 0.02	3.56 $\pm$ 0.28 *** <sup>b</sup>	2.99 $\pm$ 0.51 <sup>a</sup>	4.22 $\pm$ 0.32 *** <sup>b</sup>
WBC(T/mm <sup>3</sup> )	22.66 $\pm$ 2.05	30.11 $\pm$ 1.0 ***	29.10 $\pm$ 4.8 8	24.15 $\pm$ 4.3 0**	20.11 $\pm$ 1.0 1*** <sup>#</sup>	25.18 $\pm$ 0.1 1**
PCV(mm)	8.71 $\pm$ 0.83	13.12 $\pm$ 0.2 0***	9.56 $\pm$ 2.75 *** <sup>a</sup>	10.52 $\pm$ 0.8 5*** <sup>c</sup>	11.43 $\pm$ 1.0 * <sup>#</sup>	9.01 $\pm$ 1.05 *** <sup>b</sup>
Lymphocytes(%)	40.32 $\pm$ 0.19	60.13 $\pm$ 0.0 2***	55.31 $\pm$ 0.9 5*** <sup>a</sup>	50.42 $\pm$ 2.2 7*** <sup>c</sup> <sup>\$</sup>	49.50 $\pm$ 0.0 5*** <sup>#</sup> <sup>d</sup>	57.40 $\pm$ 1.5 3*** <sup>b</sup>
Monocytes(%)	2.00 $\pm$ 0.10	2.53 $\pm$ 0.45 ***	1.03 $\pm$ 0.06 *** <sup>a</sup>	1.00 $\pm$ 0.09 ***	1.12 $\pm$ 0.10 *** <sup>#</sup>	1.10 $\pm$ 0.10 *** <sup>b</sup>
Neutrophils(%)	47.64 $\pm$ 1.96	55.12 $\pm$ 0.1 1***	51.00 $\pm$ 0.4 9*	49.45 $\pm$ 0.2 9*** <sup>a</sup> <sup>\$</sup>	50.24 $\pm$ 2.1 0**	52.58 $\pm$ 0.6 4
Platelets (lakhs/mm <sup>-3</sup> )	2.10 $\pm$ 1.11	1.65 $\pm$ 1.41 ***	1.70 $\pm$ 0.51 *	1.55 $\pm$ 1.21 *** <sup>\$</sup>	1.43 $\pm$ 2.10 **	1.69 $\pm$ 0.84 ***

\*\*\* p < 0.001 was found significant of Normal control v/s EAC disease control, <sup>a</sup> p < 0.001 was found significant of AgNPs loaded ME v/s EAC disease control, <sup>b</sup> p < 0.001 was found significant of EAC control v/s Mtx, \*\* p < 0.01 was found significant of AgNPs in BNCs v/s EAC disease control, <sup>c</sup> p < 0.001, \*\*p < 0.01, \* p < 0.05, AgNPs in BNCs v/s Mtx, \* p < 0.05 was found significant of GANPs v/s Mtx, <sup>#</sup> p < 0.001 GANPs v/s EAC disease control, <sup>d</sup> p < 0.001 GANPs v/s Mtx, <sup>\$</sup> p < 0.001 was found significant of AgNPs in BNCs v/s EAC disease control

### 7.3 Effect on Biochemical parameters

The level of SGOT and SGPT serum enzymes were found lower than the normal control in comparison to the EAC control group (Table 6.18). The increased level of these enzymes in the bloodstream indicates damage of the organ and toxicity to blood cells. AgNPs loaded ME and AgNPs in BNCs treated groups significantly reduce these enzymes as like normal mice and standard in compared to EAC control (Table 6.18). An elevated level of SGPT in GANPs treated group indicated the sign of the liver damage. AgNPs loaded ME and AgNPs in BNCs treated groups exhibit no significant changes in ALT or SGPT levels. It indicates that liver's substantial damage and toxicity was significantly decreased after giving AgNPs loaded ME and AgNPs in BNCs oral administration in

compared to the GANPs. The biochemical analysis data (Table 6.18) shows that creatinine levels were significantly enhanced in the EAC disease control group due to impaired kidney function resulted from rapid tumor cell proliferation compared to the positive or normal control. A significant decline in creatinine levels was noticed after their treatment with AgNPs loaded ME and AgNPs in BNCs to be close to the standard group treated with Methotrexate. GANPs treatment also normalizes the level of creatinine but less than AgNPs loaded ME and AgNPs in BNCs. The analysis of liver antioxidant parameters, GSH and SOD were found lower in EAC solid tumor groups compared to normal control (Table 6.18). GSH and SOD parameters were significantly decreased due to diminished immune activity and enhanced the risk of growth of tumor cells. Treatment with AgNPs loaded ME and AgNPs in BNCs diminished the solid tumor weight and therefore decrease the oxidative stress as similar in normal mice and standard manifested by restoring the level of GSH and SOD in liver cells (Sreelatha et al., 2011). GANPs treated group also improves the level of GSH and SOD in low amount in compared to AgNPs loaded ME and AgNPs in BNCs treatment groups. No liver toxicity was observed after treatment with AgNPs loaded ME and AgNPs in BNCs regarding the elevated ALP enzymes in EAC control mice (Table 6.18). The results confirmed that total protein levels were found increasing in EAC disease control group. The oral administration of AgNPs loaded ME and AgNPs in BNCs restore the protein count as close to the normal control and standard Methotrexate group (Table 6.18). It was found that the liver and kidney functions improved after treatment with AgNPs loaded ME and AgNPs in BNCs with reduction of the oxidative stress. The therapeutic effects of oral administration of AgNPs loaded ME and AgNPs in BNCs is superior to GANPs.

Table 6.18 *Biochemical Parameters of Untreated and Treated Animals.*

<b>Parameter s</b>	<b>Normal control</b>	<b>EAC disease control</b>	<b>AgNPs loaded ME</b>	<b>AgNPs in BNCs</b>	<b>GANPs</b>	<b>Mtx</b>
SGOT(U/L )	89.56±0. 9752	135.85±3. 94***	104.37±3. 9*** a e	99.80±2.3 5*** \$	83.15±2.1 0*** # d	94.63±1.3 2*** b
SGPT(U/L )	43.30±1. 66	59.97±0.5 0***b	51.07±0.5 5*** a e	56.79±3.3 9** c	61.22±1.3 4 d	38.69±1.2 1***b
Creatinine( mg/dl)	1.38±0.1 3	3.02±0.91 ***	1.93±0.39 ***a	1.73±0.28 ***\$	1.79±0.23 ***#	1.94±0.07 b
GSH(nmol/ml)	20.10±1. 00	5.26±0.22 ***	10.17±1.7 1*** a	12.21±2.7 7*** \$	9.10±0.80 ***#	9.54±0.01 7 b
SOD(U/ml )	5.13±1.0 0	1.89±0.54 ***	3.56±0.55 *** a	2.44±0.26 c	2.54±0.48 d	3.68±0.30 b
Total Protein(g/d l)	6.38±1.1 5	7.12±1.12 ***	5.86±1.20 *** a	6.12±2.12 c	5.22±1.55 d	7.22±1.01 b
ALP(U/L )	91±1.00	142.60±1. 02***	103.20±2. 12*** a	109.50±0. 92*** \$	112.90±1. 11*** #	121.60±2. 12 b

Data was shown as (n=6., mean±SD). \*\*\* p < 0.001; p < 0.001 was found significant of Normal control v/s EAC disease control; <sup>a</sup> p < 0.001 was found significant of AgNPs loaded ME v/s EAC control; <sup>b</sup> p < 0.001 was found significant of EAC control v/s Mtx; \*\* p < 0.01 was found significant of AgNPs in BNCs v/s EAC disease control; <sup>c</sup> p < 0.001, \*\*p < 0.01, \* p < 0.05, AgNPs in BNCs v/s Mtx, \* p < 0.05 was found significant of GANPs v/s Mtx; <sup>#</sup> p < 0.001 was found significant of GANPs v/s EAC disease control; <sup>d</sup> p < 0.001 GANPs v/s Mtx; <sup>\$</sup> p < 0.001 was found significant of AgNPs in BNCs v/s EAC disease control; <sup>e</sup> p < 0.001 was found significant of AgNPs loaded ME v/s Mtx

#### 7.4 Histopathological analysis

The liver tissue of normal control showed normal hepatic lobules, narrow blood sinusoids and foci (arrow) of hepatocytes (Figure 6.41a). Liver tissue of EAC control group showed (Figure 6.41b), severe necrosis, cells filtration, large carcinoma cells, severely congested sinusoids, degeneration of hepatocytes and loss of cell boundaries (arrow) were observed. However, after their treatment with AgNPs loaded ME and AgNPs in BNCs (Figure 6.41c and d) showed the very few areas of congestion, no cell filtration, hepatic lobules and the activated Kupffer cells (arrow) were noticed like normal control (Figure 6.41a) and Methotrexate treated group (Figure 6.41f). There was no necrosis, EAC invasion or metastatic foci inside the liver in compared to EAC control group. GANPs treated EAC control mice (Figure 6.41e) shows the area of sinusoidal congestion, hepatic

lobe (arrow) that appear less like normal, some hepatic cell death observed with hydropic and ballooning degeneration in compare to AgNPs loaded ME and AgNPs in BNCs treated groups, but the severity is less than EAC control (Figure 6.41b).

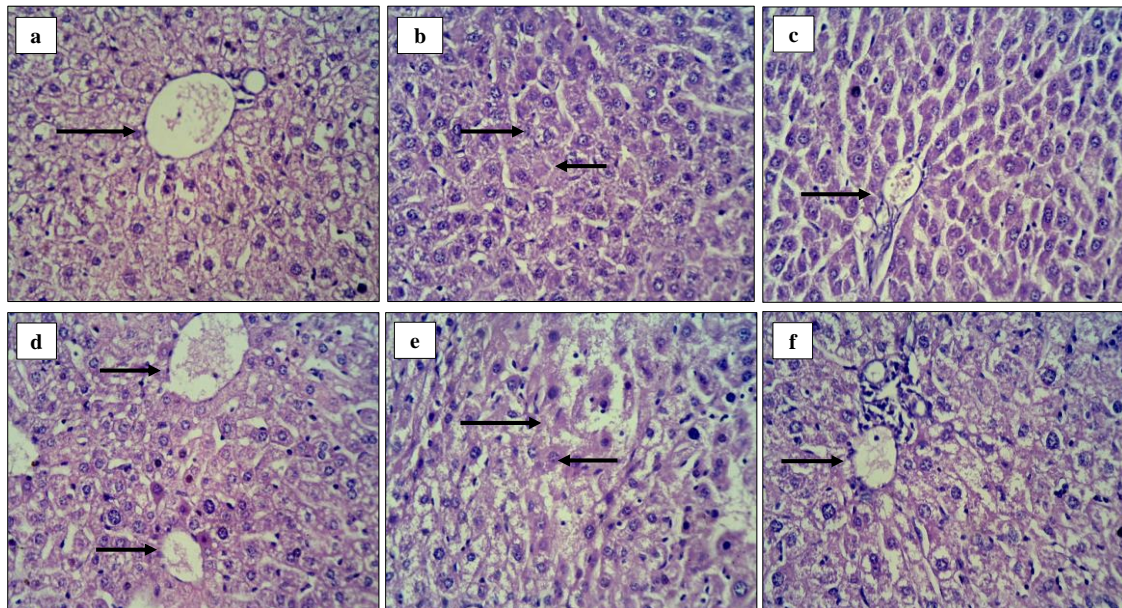


**Figure 6.41.** Histopathological examination of liver tissue (H&E $\times$ 400) of (a) Normal control, (b) EAC disease control, (c) 100 mg/kg BW of AgNPs loaded ME treated, (d) 100 mg/kg of BW of AgNPs treated, (e) 100 mg/kg of BW of GANPs treated and (f) Mtx treated mice; 2.5 mg/kg BW.

The histopathological study of kidney tissue of normal control mice shows a cortex consisting of proximal convoluted tubules and distal convoluted tubules (arrow) with renal corpuscle and renal tubules (Salem, Shoukry, Teleb, Abdel-Daim, & Abdel-Rahman, 2016), (Figure 6.42a). EAC control mice showed severe congestion, necrosis, degeneration of hepatic cells and inflammatory or perivascular cell infiltration in the interstitial regions (long arrow) (Salem et al., 2016) (Figure 6.42b). The renal corpuscles functional unit of kidney show severe congestion, necrosis, loss of cell boundary and hyper cellularity (short arrow) (Navarro et al., 1999)(Kapoor et al., 2014). AgNPs loaded ME and AgNPs in BNCs treated EAC-bearing mice shows no congestion, necrosis, no inflammatory reactions and the corpuscle and tubules of nephron appear like normal kidney structure and Methotrexate treated group (Figure 6.42c and d) as compared to EAC control. Pure drug NPs showed mild congestion, necrosis and degeneration (arrow) of some renal tubules (Figure 6.42e) in compare to AgNPs loaded ME and AgNPs in BNCs treated groups. The renal corpuscles

and tubules in Methotrexate-treated EAC control mice were observed like the normal control (Figure 6.42f).

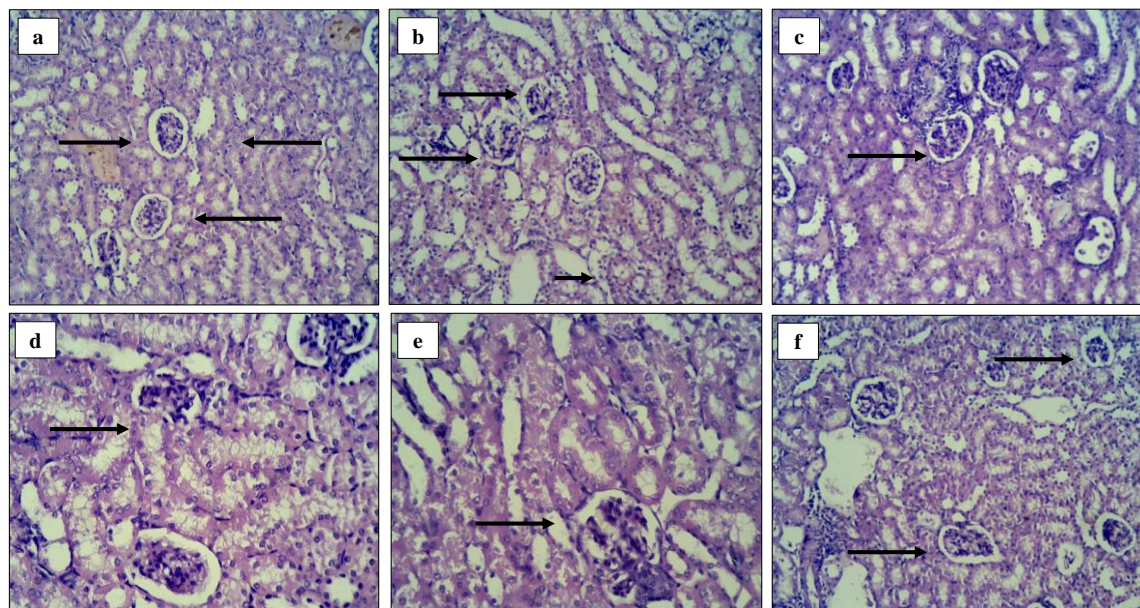


**Figure 6.42.** Histopathological examination of Kidney tissue (H&E  $\times 400$ ) of (a) Normal control, (b) EAC disease control, (c) 100 mg/kg of BW of AgNPs loaded ME treated, (d) 100 mg/kg of BW of AgNPs treated, (e) GANPs treated; 100 mg/kg BW, (f) Methotrexate(Mtx) treated mice; 2.5 mg/kg BW.

The microscopic analysis of EAC solid tumor showed a high grade of tumor cells with well-metamorphosed carcinoma encircled by a thin layer of fibrous muscles with adjacent skeletal muscle fibers (arrow). The adjoining lymphatic tissues also found with the presence of growing cancer cells within the solid tumor (Figure 6.43a). The oral administration of AgNPs loaded ME and AgNPs in BNCs in disease control groups resulting the generation of necrosis in the center of tumor (arrow) and cancer cell death was observed deep inside the tumor area (Figure 6.43b and c) like standard Methotrexate treated group (Figure 6.43e) with the inhomogeneous growth of normal cells in the surrounding area. GANPs treated group were accompanied by mild growing tumor cells within the surrounding muscle fibers (arrow) with lacking any symptoms of necrosis (Figure 6.43d) in comparison to AgNPs loaded ME and AgNPs in BNCs treated groups, but the severity is less than EAC control group. It is concluded that, AgNPs loaded ME and AgNPs in BNCs treated groups declined the solid tumor burden with number of cell division and induced apoptosis.

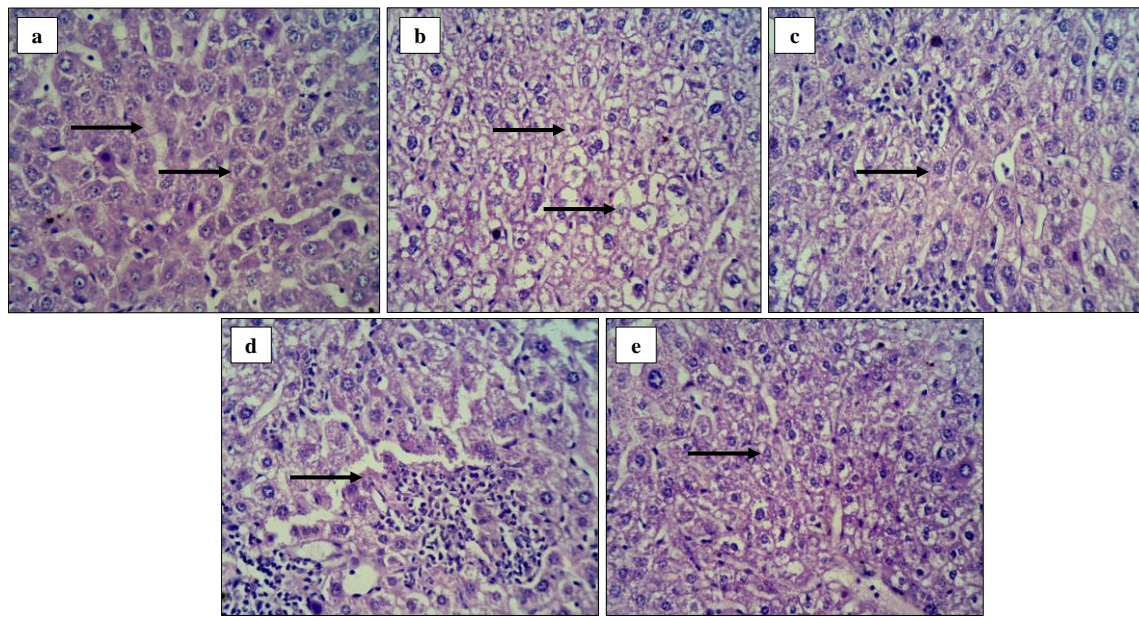


**Figure 6.43.** Histopathological examination of Solid tumor tissue (H&E  $\times 400$ ) of (a) Normal control, (b) EAC disease control, (c) 100 mg/kg BW of AgNPs loaded ME treated, (d) 100 mg/kg BW of AgNPs treated, (e) GANPs treated; 100 mg/kg BW, (f) Methotrexate(Mtx) treated mice; 2.5 mg/kg BW.

## 8 Stability study

### 8.1 Stability study of optimized AgNPs in BNCs formulation

The macroscopic observation of AgNPs indicated no evidence of precipitation or agglomeration observed over the period of three months. The optimized AgNPs formulation was subjected to particle size analysis, zeta potential and drug content evaluation which are very critical parameters in deciding the stability of the nanoparticles. The formulation retained the particle size (from  $68.06 \pm 0.25$  to  $68.12 \pm 0.25$  nm) with minor variation until three months. There is a slight decrement in zeta potential (from  $-32 \pm 0.25$  to  $-43.2 \pm 4.20$  mV) until three months due to temperature effects. As the temperature increases the zeta potential value decreased. There is no variation in drug content (from  $95.23 \pm 0.25$  to  $95.13 \pm 0.40\%$ ) with minor variation until three months. The study suggests that AgNPs in BNCs formulation is stable at high temperature. The use of a stabilizer, starch might have an important role in achieving the stability of the formulations. Table 6.19 represents the particle size, surface charge and GA content of AgNPs at 40 °C and 75%  $\pm$  5% RH during the stability period. It is concluded that AgNPs in BNCs systems is indicating good physical stability throughout the test.

Table 6.19 *Physical Stability Parameters of Optimized AgNPs Formulation. Data was presented as mean $\pm$ SD; n=3*

<b>Evaluation Parameters</b>	<b>Months</b>			
	<b>0</b>	<b>1</b>	<b>2</b>	<b>3</b>
<b>Particle size(nm)</b>	68.06 $\pm$ 0.25	68.06 $\pm$ 0.50	68.08 $\pm$ 0.21	68.12 $\pm$ 0.25
<b>Zeta potential(mV)</b>	-32 $\pm$ 0.25	-40.8 $\pm$ 5.16	-41.8 $\pm$ 5.16	-43.2 $\pm$ 4.20
<b>Drug Content (%)</b>	95.23 $\pm$ 0.25	95.23 $\pm$ 0.88	95.03 $\pm$ 1.35	95.13 $\pm$ 0.40

## 8.2 Stability study of optimized AgNPs loaded ME formulation

The macroscopic observation of AgNPs loaded ME indicated no evidence of phase separation or any precipitation or flocculation observed because of Brownian movement of the microemulsion droplets. Centrifugation study was studied to determine the impact of gravitational force on AgNPs loaded ME. No phase segregation was observed in formulation after centrifugation at 3500 rpm for 30 min which suggests that particles has a good stability (Table 6.20). There was no phase segregation identified after three freeze-thaw cycles and six heating cooling cycle indicating a thermal stability of the optimized AgNPs loaded ME (Table 6.20). Table 6.21 lists the physical stability of AgNPs loaded ME formulation at a temperature of 40 $\pm$  2°C, 75 $\pm$ 5% RH for 90 days. The stability showed that the microemulsion system remained homogenous up to 90 days even at temperature of 40°C. There was no major growth observed (from 25.71 $\pm$ 1.70 to 30.95 $\pm$ 0.70nm) in the droplet size over a period of 90 days storage. The negative charge distribution of particles showed the stability of microemulsion over the period of the storage time. Drug content of AgNPs loaded ME was found to be slightly decreased from 95.23  $\pm$  0.25 to 92.00  $\pm$  1.50 % within 3 months with no significant change in the chemical composition of the formulation. It is concluded that AgNPs loaded ME systems are indicating good physical stability throughout the test.

Table 6.20 *Thermodynamic Stability Study of AgNPs loaded ME Formulation*. Data was presented as mean $\pm$ SD; n=3

Thermodynamic stability parameters				
<b>Centrifugation (3500rpm)</b>	++			
<b>Temperature(°C)</b>	4 45	4 45	4 45	4 45
<b>Heating cooling cycle (six cycles)</b>	++ ++	++ ++	++ ++	++ ++
<b>Temperature(°C)</b>	-20 25	-20 25	-20 25	-20 25
<b>Freeze thaw cycle (three cycles)</b>	++ ++	++ ++	++ ++	++ ++

++: No phase separation

Table 6.21 *Physical Stability Study of Optimized AgNPs loaded ME Formulation*. Data was presented as mean $\pm$ SD; n=3

Evaluation Parameters	0 day	30 <sup>th</sup> day	60 <sup>th</sup> day	90 <sup>th</sup> day
<b>Globule size(nm)</b>	25.71 $\pm$ 1.70	28.41 $\pm$ 1.51	30.42 $\pm$ 1.90	30.95 $\pm$ 0.70
<b>Zeta potential(- mV)</b>	0.361 $\pm$ 0.41	0.45 $\pm$ 6.71	0.48 $\pm$ 0.13	0.57 $\pm$ 0.13
<b>Drug Content (%)</b>	95.23 $\pm$ 0.25	94.83 $\pm$ 0.20	94.8 $\pm$ 0.35	92 $\pm$ 1.50
<b>Phase separation</b>	No	No	No	No

## SUMMARY

- In this research, we developed a pharmaceutical dosage form with inducing therapeutic effectiveness against MCF-7 breast cancer cell line and EAC solid tumor animal model.
- Gallic acid was used as a main component.
- The Gallic acid was evaluated for its physicochemical properties.
- Silver nanoparticles was synthesized in bio-nanocomposites and optimized by Artificial neural network modelling (ANN) using MATLAB 2013.
- The final optimized silver nanoparticles were evaluated for various parameters like particle size, shape and surface morphology, zeta potential and entrapment efficiency.
- The optimized AgNPs was also evaluated drug release in *in vitro*. AgNPs in BNCs system exhibit the significant drug release in the acidic pH of MCF-7 cancer cells which increases bioavailability and therapeutic concentration of drug to cancer cells compared to healthy cells.
- Silver nanoparticles loaded Microemulsion (AgNPs loaded ME) was synthesized and optimized by D-optimal mixture design using Design expert software.
- The final optimized AgNPs loaded ME formulation was evaluated for physicochemical parameters (viscosity, pH, conductivity, refractive index, surface tension and drug content,), particle shape and surface morphology, zeta potential.
- AgNPs loaded ME system exhibit the significant drug release in the acidic pH of MCF-7 cancer cells due to their pH sensitive property which increases drug bioavailability and therapeutic concentration of drug to breast cancer cells compared to healthy cells.
- The results indicated that the small size AgNPs synthesized in BNCs and AgNPs loaded ME have promising antibacterial potential against microorganisms. Binding of AgNPs to microbial cell surface membrane depends on the surface area of nanoparticles. Small particles having large surface area will have a potential bactericidal effect and disturb its function, such as permeability and respiration than larger particles.
- From the morphological analysis of AgNPs loaded ME and AgNPs treated cancer cells structural changes like cell contraction, changes in membrane surface and inhibition of cell growth was observed. It was confirmed that apoptosis has been induced in treated MCF-7 cancer cells in compared to control.

- The analysis of hematological and biochemical parameters and histopathological study were carried out to evaluate the effectiveness of formulation in the systematic circulation and on the function of the perfused organs. From the *in vivo* results in the mice model it was observed that AgNPs in BNCs and AgNPs loaded ME was able to breast cancer in animal model. These can easily target the breast cancer cells and hence able to release the drug for prolonged period without affecting normal cells.
- From the stability studies, it was proved that AgNPs in BNCs and AgNPs loaded ME are stable at high temperature with retained their therapeutic potential.

## CONCLUSION

In this present investigation, AgNPs was synthesized in the bentonite/starch bio-nanocomposites (BNCs) and in AOT microemulsion system by using Gallic acid (GA) reduction aiming at studying their anticancer activity against BC cell line (*in vitro*) and animal model (*in vivo*). The Artificial neural network model and D-optimal mixture design have been used for the optimization and evaluation of independent factors in respect to response variables affecting AgNPs synthesis in BNCs and in ME respectively. The physicochemical characterization confirmed the formation of AgNPs in BNCs and AgNPs loaded ME. *In vitro* release study confirmed that optimized formulation increases bioavailability and therapeutic effectiveness of Gallic acid in targeted cancer cells in comparison to healthy cells. This research also showed the potential antibacterial activity of AgNPs in BNCs and AgNPs loaded ME against pathogenic bacteria's and fungus. Cytotoxicity study of the AgNPs in BNCs and AgNPs loaded ME microemulsion against MCF-7 cancer cell lines implies that they can be utilized as a prospective anticancer agent for treating BC. The *in vivo* study and the microscopic analysis confirmed the effective drug delivery and the significant therapeutic productivity of the AgNPs in BNCs and AgNPs loaded ME formulations with an inducing apoptosis and necrosis in the tumor cells with lack of inducing poisonous side effects to the other body organs. Therefore, the prepared AgNPs in BNCs and AgNPs loaded ME formulations can used as a successful oral delivery carrier on a solid breast carcinoma. Thus, AgNPs in BNCs and AgNPs loaded ME considered a promising antitumor agent for both cell line and solid tumor in mice models.

## **FUTURE PERSPECTIVES**

Breast cancer is the pervasive disease in females all over the globe. It is reported in various research that the treatment of breast cancer using proved management like chemotherapy and radiotherapy exhibits the strong side effects especially when it is used over a long period and develops the drug resistance. Therefore, there is strong need to develop the nanocarrier dosage form which enhance the therapeutic effects of the anticancer medicines to the target tumor cells without attacking normal cells. It can be used after future implication of clinical analysis. The designed formulation represents the controlled action of drug at a breast cancer cells with improved bioavailability of anticancer drug at a target site without affecting normal cells. The formulated AgNPs in bio-nanocomposites and AgNPs loaded microemulsion proved to be suitable for oral controlled drug with improved drug loading capacity and stability throughout the storage period without losing therapeutic potential. These formulations will also solve the problem of drug hostility to the cancer patients and increased the uptake of antitumor drugs to the cell membranes. These two formulations increased the target specificity with low dose administered with sparing healthy tissue by protecting them from enzymatic degradation and increase patient compliance. In future, after conducting some more clinical research, these formulations can prove to be safe, non-toxic to healthy cells and cheaper as compared to existing dosage forms.